Contribution from the Departments of Chemistry and Physics, Monash University, Clayton, Victoria 3168, Australia, and School of Chemistry, University of Western Australia, Nedlands, WA 6009, Australia

Variable-Temperature Magnetic, Spectral, and X-ray Crystallographic Studies of "Spin-Crossover" Iron(III) Schiff-Base–Lewis-Base Adducts. Influence of Noncoordinated Anions on Spin-State Interconversion Dynamics in [Fe(salen)(imd)$_2$]Y Species (Y = ClO_4^-, BF_4^-, PF_6^-, BPh_4^-; imd = Imidazole)

Brendan J. Kennedy,[1a] Anthony C. McGrath,[1b] Keith S. Murray,*[1a] Brian W. Skelton,[1c] and Allan H. White[1c]

Received May 29, 1986

A detailed variable-temperature magnetic, spectral, and structural study has been made on a wide range of polycrystalline Fe^{III} Schiff-base complexes of type [Fe(Schiff base)$(L)_2$]Y, where Schiff base = dianions of *N,N'*-ethylenebis(salicylaldimine) (salen), *N,N'*-ethylenebis(3-methoxysalicylaldimine) (3MeO-salen), *N,N'*-ethylenebis(3-ethoxysalicylaldimine) (3EtO-salen), *N,N'-o*-phenylenebis(salicylaldimine) (saloph), *N,N'*-ethylenebis(acetylacetone) 2,2'-imine (acen), *N,N'*-ethylenebis(benzoylacetylacetone) 2,2'-imine (benzacen), L = imidazole (imd) or pyrazole (pyz) base, and Y = ClO_4^-, BF_4^-, PF_6^-, BPh_4^-. Variation in the various components of the complex yield spin states such as pure high spin, pure low spin, and spin crossover ($^5/_2 \rightleftharpoons {}^1/_2$). Magnetic susceptibilities and ESR and Mössbauer spectra show that some of the crossover systems are of the continuous/complete type (as defined by P. Gütlich) while others are incomplete. The dependence of the crossover transformation on variation in the noncoordinated anions, Y, was probed in depth in the [Fe(salen)$(imd)_2$]Y series. The Y = ClO_4^- example shows a complete spin crossover, with a rate of spin transformation greater than 10^{-7} s as judged by the observation of a single "averaged" quadrupole doublet in the Mössbauer spectrum at high temperatures and a single low-spin doublet at low temperatures. This compound therefore provides another example of the small number of known Fe{N_4O_2} complexes exhibiting rapid spin transformation dynamics. Crystal structure determinations at 295 and 120 K, temperatures on each side of the crossover region, reveal the essentially high-spin "Fe-ligand" dimensions at 295 K and the low-spin dimensions at 120 K. Comparisons with the 295 K crystal structures of the Y = BF_4^- (crossover) and Y = PF_6^- (high spin) complexes show subtle structural differences, such as imidazole ligand orientations, equatorial ligand/imidazole C–H interactions, and Fe{NCH_2CH_2N} ring conformations (i.e. "envelope" in $^5/_2 \rightleftharpoons {}^1/_2$, "meso" in $^5/_2$), which probably contribute to the spin-state differences. Crystal data: Y = ClO_4^-, 120 K (**1a**), orthorhombic, $P2_12_12_1$, $Z = 4$, $a = 15.411$ (7) Å, $b = 13.328$ (7) Å, $c = 11.149$ (4) Å, $V = 2290$ (2) Å^3, refinement to $R = 0.063$ and $R' = 0.080$; Y = ClO_4^-, 295 K (**1b**), orthorhombic, $P2_12_12_1$, $Z = 4$, $a = 15.556$ (6) Å, $b = 13.495$ (6) Å, $c = 11.468$ (4) Å, $V = 2407$ (2) Å^3, refinement to $R = 0.050$ and $R' = 0.047$; Y = BF_4^- (**2**), orthorhombic, $P2_12_12_1$, $Z = 4$, $a = 15.490$ (3) Å, $b = 13.357$ (3) Å, $c = 11.472$ (2) Å, $V = 2374$ (1) Å^3, refinement to $R = 0.059$ and $R' = 0.037$; Y = PF_6^- (**3**), triclinic, $P\bar{1}$, $Z = 2$, $a = 13.573$ (3) Å, $b = 10.392$ (3) Å, $c = 10.310$ (3) Å, $\alpha = 65.35$ (2)°, $\beta = 88.55$ (2)°, $\gamma = 76.74$ (2)°, refinement to $R = 0.047$ and $R' = 0.039$.

Introduction

We have recently described spin-crossover transformations in a range of d^7 cobalt(II) systems of type Co(salen)L, where $salen^{2-}$ = *N,N'*-ethylenebis(salicylaldiiminato) dianion and L = imidazole type base.[2] The emphasis in that study was on how chemical, structural, and bonding effects within the molecular species influenced the crossover phenomenon, although it was recognized that intermolecular solid-state effects were also important. A similar approach has been adopted in the present paper, in which we describe variable-temperature crystal structures, magnetic susceptibilities, and Mössbauer and ESR spectra for a range of six-coordinate d^5 iron(III) Schiff-base complexes of type [Fe(X-salen)$(L)_2$]Y, where X-salen is a ring-substituted or unsubstituted {O_2N_2} chelate, L is an imidazole or pyrazole base, and Y = ClO_4^-, BF_4^-, PF_6^-, BPh_4^- (Figure 1). Spin-crossover effects were first recognized in these complexes by Nishida et al.[3,4] in a semiquantitative way; we have extended considerably the number of physicochemical probes, the range of temperature covered (i.e. 4.2–300 K), and the structural knowledge on these species. Contemporaneous with the present work[5] have been the related studies by Hendrickson et al.[6-9] on bis(tridentate) [Fe(salAPA)$_2$]Y complexes (where $salAPA^-$ = Schiff base from salicylaldehyde and (aminopropyl)aziridine), by Maeda et al.[10,11] on [Fe(acen)(R-py)$_2$]Y (where $acen^{2-}$ = *N,N'*-ethylenebis(acetylacetone) 2,2'-imine dianion and R-py = substituted pyridine), and by Matsumoto et al.[12] on quinquedentate derivatives of type [FeA(X)]$^{n+}$ (where A^{2-} = 4-azaheptamethylene-1,7-bis(salicylideneamine) dianion and X = pyridine or imidazole base or Cl^-, N_3^-, etc). Earlier studies by Hendrickson et al.[13,14] on bis(tridentate) [Fe(sal-Een)$_2$]$^+$ complexes (where sal-Een = Schiff base from salicylaldehyde and *N*-ethylethylenediamine), by Wilson, Sinn, et al.[15] on hexadentate [Fe(sal)$_2$trien]$^+$ complexes, and by Zelentsov et al.[16] on bis(tridentate) [Fe(X-thsa)$_2$]$^-$ species (where X-thsa = ring-substituted salicylaldehyde thiosemicarbazone possessing a {SNO} donor group) are also relevant. Six-coordinate iron(III) porphyrin complexes such as [Fe(OEP)(3Cl-py)$_2$]ClO_4 also exhibit crossover behavior similar to that observed in the present salen series, and a detailed magnetostructural investigation on this system has recently been made by Scheidt and co-workers.[17-19] Such studies are important in attempting to understand

(1) (a) Department of Chemistry, Monash University. (b) Department of Physics, Monash University. (c) University of Western Australia.
(2) Kennedy, B. J.; Fallon, G. D.; Gatehouse, B. M. K. C.; Murray, K. S. *Inorg. Chem.* **1984**, *23*, 580.
(3) Nishida, Y.; Oshio, S.; Kida, S. *Chem. Lett.* **1975**, 79.
(4) Nishida, Y.; Oshio, S.; Kida, S. *Bull. Chem. Soc. Jpn.* **1977**, *50*, 119.
(5) Brain, G.; Kennedy, B. J.; Murray, K. S. Presented at the COMO 12 Conference of the Royal Australian Chemical Institute, Hobart, Tasmania, Jan 1984; Abstract PII-35. Kennedy, B. J. Ph.D. Thesis, Monash University, 1984.
(6) Federer, W. D.; Hendrickson, D. N. *Inorg. Chem.* **1984**, *23*, 3861.
(7) Federer, W. D.; Hendrickson, D. N. *Inorg. Chem.* **1984**, *23*, 3870.
(8) Timken, M. D.; Strouse, C. E.; Soltis, S. M.; Daverio, S. R.; Hendrickson, D. N.; Abdel-Mawgoud, A. M.; Wilson, S. A. *J. Am. Chem. Soc.* **1986**, *108*, 395.
(9) Timken, M. D.; Abdel-Mawgoud, A. M.; Hendrickson, D. N. *Inorg. Chem.* **1986**, *25*, 160.
(10) Maeda, Y.; Ohshio, H.; Takashima, Y. *Chem. Lett.* **1982**, 943.
(11) Ohshio, H.; Maeda, Y.; Takashima, Y. *Inorg. Chem.* **1983**, *22*, 2684.
(12) Matsumoto, N.; Ohta, S.; Yoshimura, C.; Ohyoshi, A.; Kohata, K.; Okawa, H.; Maeda, Y. *J. Chem. Soc., Dalton Trans.* **1985**, 2575.
(13) Haddad, M. S.; Lynch, M. W.; Federer, W. D.; Hendrickson, D. N. *Inorg. Chem.* **1981**, *20*, 123.
(14) Haddad, M. S.; Federer, W. D.; Lynch, M. W.; Hendrickson, D. N. *Inorg. Chem.* **1981**, *20*, 131.
(15) Sim, G.; Sinn, E.; Petty, R. H.; Merrill, C. L.; Wilson, L. J. *Inorg. Chem.* **1981**, *20*, 213.
(16) E.g.: Ryabova, N. A.; Ponomarev, V. I.; Zelentsov, V. V.; Atovmyan, L. O. *Sov. Phys.—Crystallogr.* (*Engl. Transl.*) **1981**, *26*, 53; **1982**, *27*, 46; **1982**, *27*, 171, and references therein.
(17) Scheidt, W. R.; Geiger, D. K.; Haller, K. J. *J. Am. Chem. Soc.* **1982**, *104*, 495.

0020-1669/87/1326-0483$01.50/0

Table I. Crystal Data for [Fe(salen)(imd)$_2$]Y Complexes

	1a	1b	2	3
anion Y	ClO_4^-	ClO_4^-	BF_4^-	PF_6^-
formula	$C_{22}H_{22}ClFeN_6O_6$	$C_{22}H_{22}ClFeN_6O_6$	$C_{22}H_{22}BF_4FeN_6O_2$	$C_{22}H_{22}F_6FeN_6O_2P$
M_r	557.8	557.8	545.1	603.3
T, K	120	295	295	295
cryst syst	orthorhombic	orthorhombic	orthorhombic	triclinic
space group	$P2_12_12_1$ (No. 19)	$P2_12_12_1$	$P2_12_12_1$	$P\bar{1}$ (No. 2)
a, Å	15.411 (7)	15.556 (6)	15.490 (3)	13.573 (3)
b, Å	13.328 (7)	13.495 (6)	13.357 (3)	10.392 (3)
c, Å	11.149 (4)	11.468 (4)	11.472 (2)	10.310 (3)
α, deg				65.35 (2)
β, deg				88.55 (2)
γ, deg				76.74 (2)
U, Å^3	2290 (2)	2407 (2)	2374 (1)	1282.5 (6)
D_{measd}, g cm^{-3}	...	1.53	1.53	1.56
D_{calcd}, g cm^{-3}	1.62	1.54	1.52	1.56
Z	4	4	4	2
$F(000)$	1148	1148	1116	614
specimen, mm	0.35 × 0.35 × 0.20	0.35 × 0.35 × 0.20	0.35 × 0.35 × 0.18	0.12 × 0.32 × 0.08
μ_{Mo}, cm^{-1}	8.2	7.8	6.9	7.0
A^*_{max}, A^*_{min}	1.27, 1.14	1.25, 1.14	1.26, 1.11	1.09, 1.05
$2\theta_{max}$, deg	77.5	60	45	45
N	7024	3597	1792	3378
N_o	4750	2414	1333	1758
R (preferred chirality)	0.063	0.050	0.059	0.047
R'	0.080	0.047	0.037	0.039

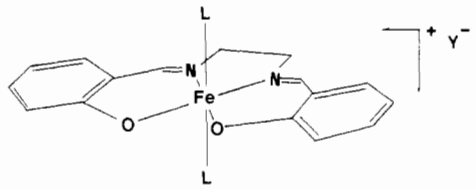

Figure 1. General structural formula of [Fe(X-salen)(L)$_2$]Y complexes (X = H, 3-MeO–, 3-EtO–; L = imidazole types base; Y = ClO_4^-, BF_4^-, BPh_4^-, PF_6^-).

spin-equilibrium phenomena in ferric heme proteins such as azidometmyoglobin,[20] cytochrome P450,[21] and cytochrome *c* peroxidase.[22]

One of the intriguing features to emerge from recent studies on iron(III) spin-crossover solid complexes is that in a number of cases the rate of interconversion between the high-spin (S = $^5/_2$) and low-spin (S = $^1/_2$) states is rapid enough on the Mössbauer time scale to be able to observe only one quadrupole doublet.[23] The spin-state interconversion rates in the Schiff-base FeN_4O_2 systems, referred to above, appear to be influenced by subtle solid-state effects and by counterion (Y) and ligand substituent changes.[8,9,11,24] We describe here similar observations within the [Fe(salen)(L)$_2$]Y complexes. In the L = imidazole series detailed X-ray crystallographic studies of the Y = ClO_4^-, PF_6^-, and BF_4^- salts at 295 K and also of the Y = ClO_4^- salt at 120 K have been made in order to try to ascertain which structural features, if any, influence the nature and dynamics of the spin-state change. The perchlorate salt displays a gradual, but complete, crossover from the high-spin to low-spin state, and so the crystal structure determination at temperatures on each side of the crossover temperatures have enabled correlations to be made with the variable-temperature magnetic and spectral data.

Experimental Section

Synthesis. Fe(salen)Cl, Fe(3MeO-salen)Cl·H_2O, Fe(3EtO-salen)Cl·H_2O, Fe(saloph)Cl, and Fe(acen)Cl were prepared by the method of Gerloch et al.[25] and recrystallized from acetone.

[Fe(salen)(imd)$_2$]ClO_4. A 0.5-g amount of Fe(salen)Cl was suspended in 25 mL of methanol, and 0.5 g of imidazole was added. The solution was refluxed for 10 min and then filtered, while hot, into a freshly prepared methanol solution (10 mL) of sodium perchlorate (0.4 g). When the mixture stood overnight, large reddish brown crystals separated, which were collected, washed with 2 × 5 mL portions of ice-cold methanol, and dried in air. Analytical data for this complex and all others are given in the supplementary material.

All other Lewis-base adducts of Fe^{III}salen and Fe^{III}saloph were prepared in a similar manner.[4]

[Fe(acen)(*N*-Me-imd)$_2$]BPh_4. This was prepared from Fe(acen)Cl in a manner identical with that described above except that the fine blue needles that separated after 1 h were collected, washed twice with 2 × 5 mL portions of ice-cold methanol, and dried in air.

[Fe(benzacen)(*N*-Me-imd)$_2$]ClO_4. A 0.42-g amount of anhydrous $FeCl_3$ was added to a hot methanol solution (20 mL) containing 0.87 g of benzacenH_2 and 1 g of *N*-methylimidazole. After it was refluxed for 20 min, the mixture was filtered, while hot, into a methanol solution of $NaClO_4$ (0.4 g in 15 mL). When this mixture stood for 4 h, fine blue/green crystals separated, which were filtered, washed with methanol, and dried.

[Fe(3-EtO-salen)(imd)$_2$]BPh_4. A 0.23-g amount of Fe(3EtO-salen)Cl·H_2O was suspended in 25 mL of methanol and 0.35 g of imidazole added. After it was refluxed for 10 min the solution was filtered, while hot, and 0.2 g of $NaBPh_4$ in 10 mL of methanol added. The volume was reduced by half, and the solution was then cooled in an ice bath for 2 h, during which time small dark purple/brown crystals were deposited. These were collected, washed with 2 × 5 mL of ice-cold methanol, and dried in air. If the solution stood in air for longer periods, appreciable amounts of the orange μ-oxo dimer [Fe(3EtO-salen)]$_2$O were produced.

All other [Fe(3MeO-salen)L$_2$]$^+$ and [Fe(3EtO-salen)L$_2$]$^+$ adducts, with L = imd or *N*-Me-imd, were prepared in a similar manner. It should be noted that for L = 5-phenylimidazole or pyrazole, and under conditions of rapid isolation, the products obtained were monobase/monoaquo species of type [Fe(3RO-salen)(L)(H_2O)]BPh_4. The properties of these high-spin species have been described elsewhere.[26]

Caution! Perchlorate salts can potentially explode during drying or grinding, so care should be exercised in handling such compounds. So far we have not experienced any problems, although only samples of less than 20 mg at a time were ground up for susceptibility measurements.

(18) Scheidt, W. R.; Geiger, D. K.; Hayes, R. G.; Lang, G. *J. Am. Chem. Soc.* **1983**, *105*, 2625.
(19) Geiger, D. K.; Lee, Y. J.; Scheidt, W. R. *J. Am. Chem. Soc.* **1984**, *106*, 6339.
(20) Messana, C.; Cerdonio, M.; Shenkin, P.; Noble, R. W.; Fermi, G.; Perutz, R. W.; Perutz, M. F. *Biochemistry* **1978**, *17*, 3652.
(21) Lange, R.; Bonfils, C.; Debye, P. *Eur. J. Biochem.* **1977**, *79*, 623.
(22) Iizuka, T.; Kotani, M.; Yonetani, M. *J. Biol. Chem.* **1971**, *246*, 4731.
(23) Rickards, R.; Johnson, C. E.; Hill, H. A. O. *J. Chem. Phys.* **1968**, *48*, 5231.
(24) Maeda, Y.; Tutsumi, N.; Takashima, Y. *Inorg. Chem.* **1984**, *23*, 2440. Maeda, Y.; Oshio, H.; Takashima, Y.; Mikurya, M.; Hidaka, M. *Inorg. Chem.* **1986**, *25*, 2958.
(25) Gerloch, M.; Lewis, J.; Mabbs, F. E.; Richards, A. *J. Chem. Soc. A* **1968**, 112.
(26) Kennedy, B. J.; Brain, G.; Horn, E.; Murray, K. S.; Snow, M. R. *Inorg. Chem.* **1985**, *24*, 1647.

Table II. Non-Hydrogen Atom Coordinates for **1a,b**

	1a			1b		
atom	*x*	*y*	*z*	*x*	*y*	*z*
			Cation			
Fe	0.19192 (5)	0.85797 (5)	0.84466 (7)	0.19914 (5)	0.86559 (6)	0.84085 (7)
			Salen Ligand			
O(11)	0.3025 (3)	0.9043 (3)	0.7982 (4)	0.3136 (2)	0.8922 (3)	0.7970 (4)
C(11)	0.3720 (3)	0.8486 (4)	0.7988 (5)	0.3800 (4)	0.8317 (5)	0.7983 (5)
C(12)	0.4539 (4)	0.8974 (4)	0.7977 (5)	0.4627 (4)	0.8720 (6)	0.8042 (5)
C(13)	0.5308 (4)	0.8428 (5)	0.8005 (6)	0.5344 (4)	0.8108 (7)	0.8055 (6)
C(14)	0.5295 (4)	0.7374 (5)	0.7973 (6)	0.5258 (4)	0.7119 (7)	0.7981 (6)
C(15)	0.4511 (4)	0.6890 (5)	0.7925 (6)	0.4445 (5)	0.6679 (5)	0.7891 (5)
C(16)	0.3719 (4)	0.7416 (4)	0.7935 (5)	0.3705 (4)	0.7277 (5)	0.7878 (5)
C(17)	0.2928 (4)	0.6849 (4)	0.7842 (5)	0.2894 (4)	0.6781 (4)	0.7815 (5)
N(18)	0.2169 (3)	0.7225 (3)	0.8023 (4)	0.2164 (3)	0.7197 (3)	0.7966 (4)
C(19)	0.1374 (4)	0.6642 (4)	0.7805 (5)	0.1342 (4)	0.6683 (4)	0.7758 (5)
O(21)	0.1639 (3)	0.9948 (3)	0.8826 (4)	0.1602 (2)	0.9962 (3)	0.8801 (3)
C(21)	0.0885 (3)	1.0272 (4)	0.9232 (5)	0.0855 (3)	1.0265 (4)	0.9220 (4)
C(22)	0.0810 (4)	1.1314 (4)	0.9492 (5)	0.0775 (4)	1.1268 (4)	0.9533 (5)
C(23)	0.0039 (4)	1.1698 (4)	0.9915 (5)	0.0028 (4)	1.1634 (5)	0.9972 (5)
C(24)	−0.0685 (4)	1.1088 (5)	1.0115 (5)	−0.0697 (4)	1.1028 (5)	1.0122 (6)
C(25)	−0.0629 (4)	1.0087 (5)	0.9856 (5)	−0.0626 (4)	1.0049 (5)	0.9826 (5)
C(26)	0.0143 (3)	0.9645 (4)	0.9426 (5)	0.0126 (3)	0.9648 (4)	0.9389 (5)
C(27)	0.0142 (3)	0.8586 (5)	0.9229 (5)	0.0136 (3)	0.8574 (5)	0.9167 (5)
N(28)	0.0794 (3)	0.8066 (3)	0.8863 (4)	0.0785 (3)	0.8088 (3)	0.8828 (4)
C(29)	0.0725 (4)	0.6965 (4)	0.8781 (5)	0.0715 (4)	0.7005 (4)	0.8698 (6)
			Imidazole Ligands			
N(31)	0.1492 (3)	0.8832 (3)	0.6790 (4)	0.1532 (3)	0.8868 (3)	0.6667 (4)
C(32)	0.0759 (3)	0.9286 (4)	0.6493 (5)	0.0805 (4)	0.9288 (4)	0.6381 (5)
N(33)	0.0680 (3)	0.9301 (4)	0.5295 (4)	0.0704 (3)	0.9273 (4)	0.5217 (4)
C(34)	0.1390 (4)	0.8830 (4)	0.4805 (5)	0.1383 (4)	0.8800 (5)	0.4755 (5)
C(35)	0.1885 (4)	0.8529 (4)	0.5737 (4)	0.1898 (4)	0.8541 (4)	0.5656 (5)
N(41)	0.2327 (3)	0.8361 (3)	1.0123 (4)	0.2357 (3)	0.8360 (3)	1.0183 (4)
C(42)	0.2431 (4)	0.9106 (4)	1.0906 (5)	0.2461 (4)	0.9062 (4)	1.0950 (5)
N(43)	0.2724 (3)	0.8765 (3)	1.1966 (4)	0.2752 (3)	0.8706 (4)	1.1970 (4)
C(44)	0.2819 (4)	0.7745 (4)	1.1864 (5)	0.2867 (4)	0.7710 (5)	1.1837 (5)
C(45)	0.2568 (4)	0.7497 (4)	1.0710 (5)	0.2612 (4)	0.7497 (4)	1.0716 (5)
			Anion			
Cl	0.16758 (8)	0.43147 (10)	0.97086 (13)	0.16609 (10)	0.43326 (11)	0.96603 (16)
O(1)	0.1225 (3)	0.4176 (4)	0.8582 (5)	0.1218 (3)	0.4185 (4)	0.8577 (5)
O(2)	0.2094 (3)	0.3398 (3)	1.0047 (5)	0.2017 (4)	0.3449 (3)	1.0051 (5)
O(3)	0.2310 (3)	0.5098 (4)	0.9571 (5)	0.2314 (3)	0.5045 (4)	0.9539 (6)
O(4)	0.1054 (3)	0.4599 (4)	1.0620 (5)	0.1034 (3)	0.4694 (4)	1.0462 (5)

Physical Measurements. Variable-temperature magnetic susceptibilities and Mössbauer and ESR spectra were obtained as described previously.[26]

Crystallography. Single crystals of $[Fe(salen)(imd)_2]ClO_4$ (**1**) and $[Fe(salen)(imd)_2]PF_6$ (**3**) were grown from the reaction mixtures described above. Crystals of the BF_4^- salt (**2**) could only be obtained in the presence of a large excess of imidazole, which cocrystallized as white crystals in conjunction with black crystals of **2**. Unique data sets were measured to the specified $2\theta_{max}$ limit with a Syntex $P2_1$ four-circle diffractometer, fitted with a graphite-monochromated Mo Kα radiation source ($\lambda = 0.7106_9$ Å) and operating in the conventional $2\theta/\theta$ scan mode. N independent reflections were measured, N_o, with $I > 3\sigma(I)$ being considered "observed" and used in the basically 9 × 9 block-diagonal least-squares refinement with statistical weights, after solution of the structure by vector methods and the application of analytical absorption correction. For the non-hydrogen atoms, anisotropic thermal parameters were refined; $(x, y, z, U_{iso})_H$ were included at estimated values. Residuals on $|F|$ at convergence, R and R', are quoted. Other conditions of data collection are summarized in Table I. Computation used the XTAL 83 computation system,[27] implemented by S. R. Hall on a Perkin-Elmer 3240 computer. Neutral-complex scattering factors were employed.[28] Ligand non-hydrogen atom numbering is as follows:

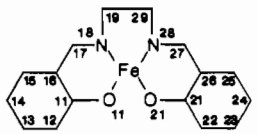

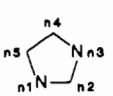

Abnormal Features. Structure **1a** was determined at ~120 K; **1b** is its room-temperature counterpart. **2** and **3** were also determined at room temperature (~295 K). The PF_6^- anion of structure **3** is disordered. **1a**, **1b**, and **2** are isomorphous. No serious extinction effects were noted in any structure.

Final vallues of non-hydrogen atom coordinates are given in Tables II and III. Non-hydrogen atom anisotropic thermal parameters for **1a**, **1b**, **2**, and **3** are given as supplementary material in Tables SUP1–4. Hydrogen atom parameters are given in Tables SUP5 and SUP6. Least-squares planes for salen ligands and imidazole rings are given in Tables SUP7 and SUP8.

Results and Discussion

Synthesis and Properties of $[Fe(X\text{-salen})(L)_2]Y$ Complexes. The synthesis of six-coordinate Lewis-base adducts from [Fe(X-salen)Cl] precursors is straightforward provided sufficient care is taken to ensure that no μ-oxo dimer, $[Fe(X\text{-salen})]_2O$, is formed during the reaction. In general, it appears that μ-oxo dimer formation is favored in the 3MeO-salen and 3EtO-salen system compared to the nonsubstituted parent complex. The rate of formation of the μ-oxo dimer in the former complexes also appears to be anion-dependent, perchlorate salts being more likely to favor μ-oxo formation than tetraphenylborate salts. The use of dry methanol as well as rapid isolation of the complexes tends to avoid contamination with μ-oxo dimer. It has not been possible to obtain pure samples of complexes containing sterically hindered bases such as 2-methylimidazole or benzimidazole despite repeated

(27) Stewart, J. M., Hall, S. R., Eds. "The XTAL System of Crystallographic Programs"; Computer Science Technical Report Series TR-901; University of Maryland, College Park, MD, 1983.

(28) Ibers, J. A., Hamilton, W. C., Eds. *International Tables for X-ray Crystallography*; Kynoch: Birmingham, England, 1974; Vol. 4.

Table III. Non-Hydrogen Atom Coordinates for **2** and **3**

	2			3		
atom	*x*	*y*	*z*	*x*	*y*	*z*
			Cation			
Fe	0.19757 (9)	0.8632 (1)	0.8434 (1)	0.18534 (8)	0.0805 (1)	0.0764 (1)
			Salen Ligand			
O(11)	0.3123 (4)	0.8916 (5)	0.7961 (5)	0.2283 (3)	−0.0916 (5)	0.0440 (5)
C(11)	0.3775 (6)	0.8293 (8)	0.7962 (8)	0.3032 (5)	−0.1348 (7)	−0.0240 (7)
C(12)	0.4624 (6)	0.8707 (10)	0.8014 (8)	0.3180 (5)	−0.2749 (7)	−0.0193 (8)
C(13)	0.5328 (6)	0.7961 (11)	0.8019 (9)	0.3941 (5)	−0.3279 (8)	−0.0859 (9)
C(14)	0.5226 (8)	0.6975 (11)	0.7959 (10)	0.4638 (5)	−0.2481 (8)	−0.1521 (8)
C(15)	0.4420 (7)	0.6605 (9)	0.7861 (11)	0.4522 (5)	−0.1105 (8)	−0.1554 (8)
C(16)	0.3706 (6)	0.7254 (8)	0.7883 (9)	0.3740 (4)	−0.0537 (7)	−0.0918 (7)
C(17)	0.2894 (7)	0.6731 (7)	0.7808 (8)	0.3655 (5)	0.0932 (7)	−0.1075 (7)
N(18)	0.2138 (5)	0.7158 (5)	0.7972 (6)	0.2986 (4)	0.1666 (5)	−0.0598 (6)
C(19)	0.1322 (7)	0.6612 (8)	0.7800 (9)	0.2931 (5)	0.3181 (7)	−0.0964 (8)
O(21)	0.1598 (3)	0.9953 (4)	0.8802 (6)	0.0763 (3)	0.0546 (5)	0.1956 (5)
C(21)	0.0852 (6)	1.0279 (7)	0.9242 (9)	0.0120 (5)	0.1423 (7)	0.2378 (7)
C(22)	0.0758 (6)	1.1305 (8)	0.9525 (8)	−0.0681 (6)	0.0924 (8)	0.3145 (9)
C(23)	0.0005 (7)	1.1670 (7)	0.9958 (9)	−0.1369 (6)	0.1784 (9)	0.3633 (9)
C(24)	−0.0716 (6)	1.1083 (8)	1.0091 (9)	−0.1274 (6)	0.3162 (8)	0.3382 (9)
C(25)	−0.0655 (6)	1.0090 (8)	0.9867 (10)	−0.0512 (6)	0.3689 (7)	0.2644 (8)
C(26)	0.0120 (6)	0.9640 (7)	0.9409 (9)	0.0207 (5)	0.2830 (7)	0.2125 (7)
C(27)	0.0122 (6)	0.8595 (8)	0.9221 (8)	0.1018 (5)	0.3448 (7)	0.1408 (7)
N(28)	0.0763 (4)	0.8060 (5)	0.8870 (7)	0.1746 (4)	0.2835 (6)	0.0862 (6)
C(29)	0.0701 (6)	0.6971 (7)	0.8761 (10)	0.2572 (5)	0.3532 (7)	0.0283 (8)
			Imidazole Ligands			
N(31)	0.1508 (4)	0.8826 (5)	0.6715 (7)	0.2949 (4)	−0.0713 (6)	0.2588 (6)
C(32)	0.0788 (6)	0.9281 (8)	0.6389 (9)	0.3550 (6)	−0.1496 (8)	0.3074 (8)
N(33)	0.0696 (5)	0.9267 (6)	0.5223 (7)	0.4071 (5)	−0.1812 (7)	0.4291 (7)
C(34)	0.1406 (6)	0.8787 (9)	0.4775 (9)	0.3793 (6)	−0.0648 (9)	0.4604 (8)
C(35)	0.1898 (6)	0.8517 (8)	0.5711 (8)	0.3093 (5)	0.0335 (8)	0.3576 (8)
N(41)	0.2349 (4)	0.8338 (5)	1.0186 (6)	0.0774 (4)	0.1842 (6)	−0.1082 (6)
C(42)	0.2462 (6)	0.9039 (7)	1.0934 (9)	−0.0216 (5)	0.2012 (8)	−0.1044 (8)
N(43)	0.2763 (5)	0.8700 (6)	1.1966 (6)	−0.0666 (4)	0.2686 (7)	−0.2338 (7)
C(44)	0.2848 (6)	0.7683 (7)	1.1834 (9)	0.0032 (6)	0.2986 (8)	−0.3306 (8)
C(45)	0.2607 (6)	0.7483 (7)	1.0758 (9)	0.0951 (5)	0.2432 (8)	−0.2511 (8)
			Anion[a]			
B,P	0.1688 (7)	0.4310 (10)	0.9691 (12)	0.3147 (2)	0.4143 (3)	0.4360 (2)
F(1)	0.1272 (4)	0.4173 (6)	0.8623 (6)	0.2794 (6)	0.5809 (7)	0.3552 (8)
F(2)	0.1978 (5)	0.3440 (5)	1.0086 (7)	0.4169 (6)	0.4309 (12)	0.3726 (10)
F(3)	0.2276 (4)	0.5021 (6)	0.9570 (8)	0.3465 (8)	0.2454 (9)	0.5200 (11)
F(4)	0.1037 (4)	0.4667 (5)	1.0396 (7)	0.3593 (10)	0.4222 (13)	0.5721 (10)
F(5)				0.2144 (7)	0.4226 (11)	0.5147 (11)
F(6)				0.2718 (9)	0.4007 (10)	0.3129 (10)
F(1′)				0.2151 (8)	0.3673 (13)	0.4259 (14)
F(2′)				0.3849 (8)	0.3045 (16)	0.3945 (16)
F(3′)				0.4117 (9)	0.4481 (12)	0.4642 (17)
F(4′)				0.2872 (12)	0.4990 (21)	0.2780 (14)
F(5′)				0.2593 (12)	0.5473 (17)	0.4475 (18)
F(6′)				0.3267 (12)	0.3056 (20)	0.5795 (14)

[a] Fluorine populations are 0.5 for **3**.

attempts using carefully dried solvents. Nonhomogeneous samples were obtained in these attempts, the exact constitutions of which have not been further explored.

The six-coordinate adducts display a large variety of colors ranging from purple/brown to blue/green. Their room-temperature magnetic moments are in the range 5.9–2.17 μ_B, consistent with the occurrence of differing spin states. The complexes with moments of ca. 5.6 μ_B are strongly thermochromic, the compound $[Fe(salen)(pyz)_2]ClO_4$, for example, changing from reddish brown at 295 K to olive green at 77 K. The low-spin state tends to be dominated by green colors. Similar thermochromic changes have been noted recently in other crossover systems.[8-12]

Dependence of the $^6A_1 \rightleftharpoons {}^2T_2$ Crossover on the Counteranion, Y, in $[Fe(salen)(imd)_2]Y$ Complexes (Y = ClO_4^-, BF_4^-, BPh_4^-, PF_6^-). Before we could investigate the influence of the in-plane Schiff base and the axial Lewis base (L) on the spin equilibrium, it was necessary to determine what influence, if any, the noncoordinated anion had on the $^6A_1 \rightleftharpoons {}^2T_2$ transition. As can be seen in Table IV, the room-temperature magnetic moments of the

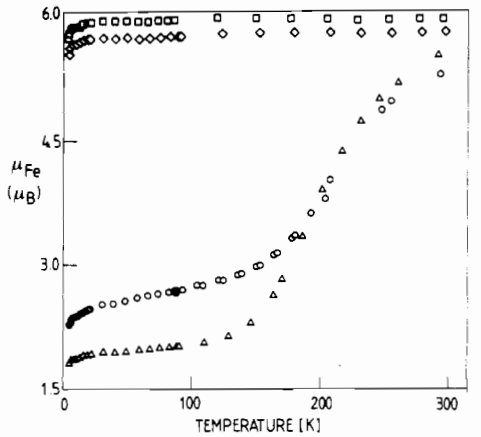

Figure 2. Magnetic moments vs. temperature for $[Fe(salen)(imd)_2]Y$ complexes: (□) Y = PF_6^-; (◇) Y = BPh_4^-; (○) Y = BF_4^-; (△) Y = ClO_4^-.

Table IV. Magnetic Moments and Spin States of Six-Coordinate Iron(III) Schiff-Base Complexes

complex	color (295 K)	μ_{eff}, μ_B	spin state
$[Fe(salen)(imd)_2]ClO_4$	brown-red	5.49	$^5/_2 \rightleftharpoons {}^1/_2$[a]
$[Fe(salen)(imd)_2]BF_4$	brown-purple	5.27	$^5/_2 \rightleftharpoons {}^1/_2$
$[Fe(salen)(imd)_2]BPh_4$	brown	5.76[b]	$^5/_2$ ($\rightleftharpoons {}^1/_2$)
$[Fe(salen)(imd)_2]PF_6$	brown	5.90	$^5/_2$
$[Fe(salen)(pyz)_2]ClO_4 \cdot H_2O$	brown-purple	5.67	$^5/_2 \rightleftharpoons {}^1/_2$
$[Fe(salen)(pyz)_2]BF_4 \cdot H_2O$	brown-purple	5.68	$^5/_2 \rightleftharpoons {}^1/_2$
$[Fe(salen)(pyz)_2]BPh_4 \cdot MeOH$	brown	5.74	$^5/_2$
$[Fe(salen)(N\text{-Me-imd})_2]ClO_4$	red-brown	5.91	$^5/_2$
$[Fe(salen)(5Cl\text{-}N\text{-Me-imd})_2]ClO_4$	brown	5.84	$^5/_2$
$[Fe(saloph)(imd)_2]ClO_4 \cdot H_2O$	olive green	5.89	$^5/_2$
$[Fe(3MeO\text{-salen})(imd)_2]BPh_4$	brown-purple	4.95[c]	$^5/_2 \rightleftharpoons {}^1/_2$
$[Fe(3MeO\text{-salen})(N\text{-Me-imd})_2]BPh_4$	brown	5.91	$^5/_2$
$[Fe(3MeO\text{-salen})(N\text{-Me-imd})_2]ClO_4$	brown-red	5.86	$^5/_2$
$[Fe(3MeO\text{-salen})(5Cl\text{-}N\text{-Me-imd})_2]ClO_4$	brown-purple	5.82	$^5/_2$
$[Fe(3EtO\text{-salen})(imd)_2]BPh_4$	brown-purple	5.58	$^5/_2 \rightleftharpoons {}^1/_2$[a]
$[Fe(acen)(N\text{-Me-imd})_2]BPh_4$	blue	5.23	$^5/_2 \rightleftharpoons {}^1/_2$[a]
$[Fe(bzacen)(N\text{-Me-imd})_2]ClO_4$	green	2.26	$^1/_2$

[a] Complete spin crossover; the other crossovers are incomplete. [b] μ_{eff} value of 5.89 μ_B reported in ref 4. [c] μ_{eff} value of 5.03 μ_B reported in ref 4.

complexes $[Fe(salen)(imd)_2]Y$, where $Y = ClO_4^-$, BF_4^-, and PF_6^-, are spread over the range 5.27–5.9 μ_B. The temperature dependence of the moments, displayed in Figure 2, show that the PF_6^- salt is high spin at all temperatures with only a small decrease at low temperature arising from zero-field splitting (ZFS) of the $^6A_1$ ground state. An acceptable fit of the data to that calculated[29] with a rhombic spin Hamiltonian for $S = {}^5/_2$ was obtained with the ZFS parameters $D = 0.6 \pm 0.1$ cm^{-1} and $E = 0.1 \pm 0.1$ cm^{-1}. Independent support for such parameter values was forthcoming in the 77 K ESR spectrum, which showed g values at 7.68 (w, sh), 4.5 (strong), and ~1.6 (w) typical of rhombically distorted Fe^{III}.

The BPh_4^- salt behaves similarly to the PF_6^- salt although the μ_{eff} value in the high-temperature region, 5.76 μ_B, while independent of temperature, is less than 5.9 μ_B, indicating the possible presence of some low-spin component. Nishida et al.[4] had previously concluded that the BPh_4^- salt was high-spin on the basis of susceptibility data obtained in the 300–80 K range.

The magnetic moments of the ClO_4^- and BF_4^- salts change markedly with temperature, the former decreasing from 5.48 μ_B at 293 K to 2.0 μ_B at ~90 K, and then slowly to 1.82 μ_B at 4.2 K. This behavior is as expected for a gradual but complete transition from the high-spin to the low-spin state with decreasing temperature. The color of the solid changes from brown-red at room temperature to olive green at 77 K. ESR spectral measurements on a powdered sample show only a broad $g \approx 4.3$ line at 295 K, changing to a strong broad line at $g = 2.13$ (with shoulders at $g = 2.27$ and 2.0) at 77 K, again compatible with a complete transition from high to low spin. The g values for the low-spin state are compatible with the unpaired electron being in the d_{xy} orbital. (The x, y directions are defined as pointing along the Fe–ligand directions.) Crystal structure determinations at 295 and 120 K, described in detail below, further confirm the spin-state change. Fitting of the experimental μ_{Fe}/T data to the theoretical model developed by Martin et al.,[30] assuming octahedral $^6A_{1g}$ and $^2T_{2g}$ states, gave quite a good fit with values of the ($^6A_{1g}$–$^2T_{2g}$) energy separation of 772 cm^{-1}; ξ (spin–orbit coupling constant) = 375 cm^{-1}, $g = 2.13$ (from the ESR spectrum), and $\log C = 2.8$ (where C is the ratio of the molecular vibrational partition function for the two spin states). The fit is shown in Figure 3. Similar parameter values were deduced recently by Maeda et al.[11] for $[Fe(acen)L_2]BPh_4$ complexes in which L = γ-picoline and 3,4-lutidine.

The magnetic behavior of the BF_4^- salt is similar to that of the perchlorate except that the μ_{Fe} values in the low-temperature region, viz. 2.6 μ_B at 80 K and 2.29 μ_B at 4.2 K, are a little higher than expected for a pure low-spin state, suggesting that the crossover is incomplete and that some high-spin form is present even at 4.2 K. Consistent with this is the observation that the powder ESR spectrum at 77 K shows a strong asymmetrical peak centered at $g \approx 2$ (with components at $g = 2.29$, 2.14, 2.00) in addition to a much weaker high-spin signal at $g = 4.3$.

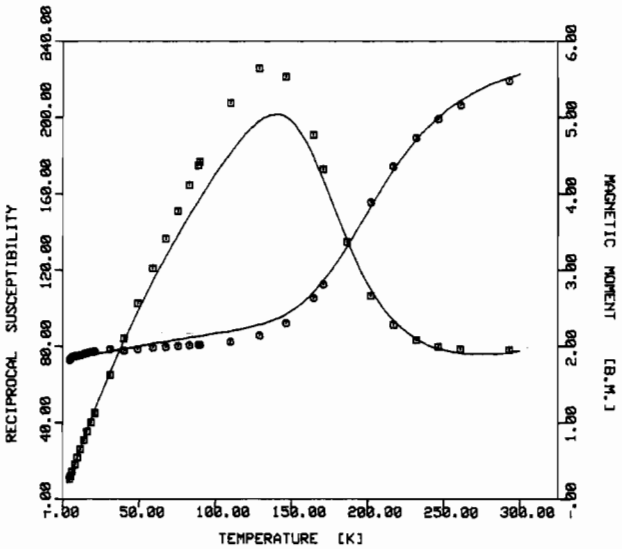

Figure 3. Magnetic moment (○) and reciprocal susceptibility (□) as a function of temperature for $[Fe(salen)(imd)_2]ClO_4$. The solid lines are the best-fit calculated values to the model of Martin et al.[30] using the parameter values given in the text.

Table V. Mössbauer Spectral Parameters for $[Fe(salen)(imd)_2]Y$ Complexes

Y	temp, K	δ,[a] mm s^{-1}	ΔE_Q, mm s^{-1}	% area	area 1/ area 2[b]	spin state
ClO_4	295	0.36	1.34	100	1.01	$^5/_2$[c]
	77	0.20	2.28	100	1.00	$^1/_2$
	4.2	0.21	2.27	100	1.00	$^1/_2$
BF_4	295	0.34	0.99	83.0	1.39	$^5/_2$
		0.34	2.51	17.0	1.00	$^1/_2$
	77	0.44	0.88	17.1	1.00	$^5/_2$
		0.20	2.27	82.9	1.00	$^1/_2$
	4.2	0.46	0.90	20.1	1.11	$^5/_2$
		0.20	2.30	79.9	1.00	$^1/_2$
PF_6	295	0.44	1.41	100	1.30	$^5/_2$
	4.2	0.64	1.57	100	2.22	$^5/_2$
BPh_4	295	0.57	1.14	100	1.54	$^5/_2$[c]
	4.2	0.48	0.96	24.8	1.18	$^5/_2$
		0.47	2.25	75.2	1.00	$^1/_2$

[a] Relative to α-Fe. [b] Area ratio of low-velocity component to high-velocity component. [c] "Averaged" spectrum.

(29) Berry, K. J.; Clark, P. E.; Murray, K. S.; Raston, C. L.; White, A. H. *Inorg. Chem.* **1983**, *22*, 3928.
(30) Ewald, A. H.; Martin, R. L.; Sinn, E.; White, A. H. *Inorg. Chem.* **1969**, *8*, 1837.

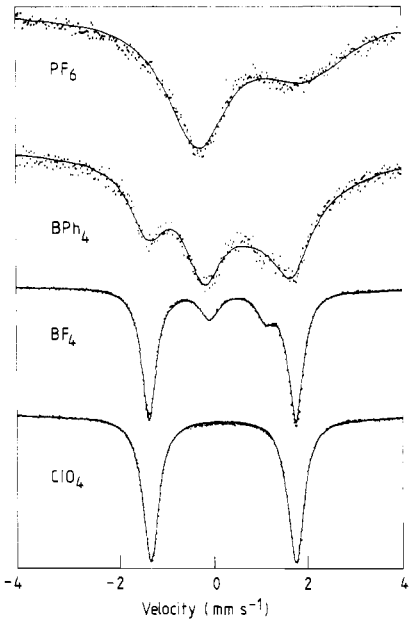

Figure 4. Zero-field Mössbauer spectra at 4.2 K of polycrystalline samples of $[Fe(salen)(imd)_2]Y$, where $Y = PF_6^-$, BPh_4^-, BF_4^-, ClO_4^-.

Mössbauer spectral measurements have proved to be particularly useful in probing the spin states in the complexes and in providing support for the magnetic susceptibility and ESR spectral data. The 4.2 K zero-field Mössbauer spectra for the four $[Fe(salen)(imd)_2]Y$ complexes are shown in Figure 4. The best-fit values of the isomer shift, δ, and quadrupole splitting, ΔE_Q, at 4.2 K and at higher temperatures are given in Table V. The broad asymmetrical doublet displayed by the PF_6^- complex is compatible with a $^6A_1$ ground state displaying very small ZFS in which population of both the excited $M_s = \pm^3/_2$ and $\pm^5/_2$ Kramers doublets and of the $M_s = \pm^1/_2$ ground doublet is occurring, even at 4.2 K, which leads to magnetic broadening. The spectrum has a similar shape at 295 K, although it is weaker, with an absorption of only ~1.0% (cf. ~2.5% at 4.2 K) due to a low Debye–Waller factor. The δ and ΔE_Q values are typical for high-spin FeN_4O_2 Schiff-base systems.[26]

The 295 K spectrum of the BPh_4^- complex is even weaker than that of the PF_6^- salt although it displays similar general features. The 4.2 K spectrum of this salt clearly shows more than one doublet, and it can be fitted to two doublets, arising from a mixture of high- and low-spin forms. The percentage area ratio of the low- and high-spin doublets is markedly at variance with the susceptibility data, which shows a predominant high-spin situation. This has also been observed before by Hendrickson et al.[13,14] on other Fe^{III} complexes and is due to differing Debye–Waller factors for the two spin states. It seems likely that the BPh_4^- salt is displaying a slow, incomplete spin crossover in which the molecules are interconverting between the low- and high-spin states slower than $\sim 10^6$ s^{-1}. Similar observations have been made for some bis(tridentate) Fe^{III} Schiff-base complexes.[13]

The Mössbauer spectra at 293, 77, and 4.2 K for the ClO_4^- salt are shown in Figure 5. The magnetic and ESR data on this complex indicate a gradual and complete spin crossover to the low-spin state when the temperature decreases to ~120 K. The Mössbauer spectrum at room temperature shows a single broad asymmetrical doublet with parameter values $\delta = 0.36$ mm s^{-1} and $\Delta E_Q = 1.34$ mm s^{-1} typical of high-spin Fe^{III}. Cooling the sample to 77 K causes a dramatic change in the appearance of the spectrum with a single well-resolved symmetrical doublet observed. The isomer shift and quadrupole splitting values of $\delta = 0.20$ mm s^{-1} and $\Delta E_Q = 2.28$ mm s^{-1} are indicative of low-spin Fe^{III}. Further cooling to 4.2 K causes no notable changes in the appearance of the spectrum. While the experimental facilities were unfortunately not available to us to be able to obtain spectra at more temperatures in the "crossover" region of 295–77 K, the results clearly show that this complex is another example of the small, known

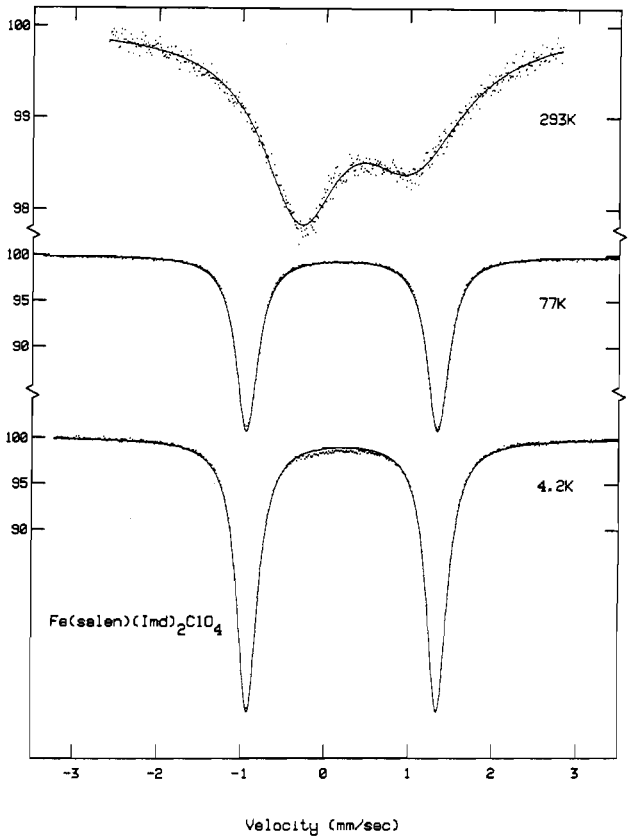

Figure 5. Mössbauer spectra of $[Fe(salen)(imd)_2]ClO_4$ at 293, 77, and 4.2 K.

group of FeN_4O_2 complexes in which the transition between the high- and low-spin states takes place at a rate faster than the inverse of the lifetime of the Mössbauer nucleus ($> \sim 10^7$ s^{-1}). Observation of just a single quadrupole doublet at higher temperatures is because the nucleus sees an average of the high- and low-spin states. Changes in the magnitude of δ and ΔE_Q with temperature are similar in general detail to those in related systems reported, during the course of the present work, by Maeda et al.[10-12,24] and Hendrickson et al.[6-9]

In contrast to the case for the ClO_4^- salt, the BF_4^- complex shows two doublets at all temperatures. The low-spin doublet is well-resolved at temperatures of 77 K and lower and is similar to that in the ClO_4^- case. As can be seen in Figure 4, the inner high-spin doublet present in ~20% area is of similar line width to the outer low-spin doublet and much narrower than the high-spin lines in the PF_6^- and BPh_4^- spectra. This difference in line width could result from an appreciable ZFS of the $^6A_1$ state in the BF_4^- complex leading to population of mainly the $M_s = \pm^1/_2$ Kramers doublet and hence to the absence of magnetic broadening. Furthermore, it seems likely that the observation of the weak high-spin doublet at 77 and 4.2 K is indicative of an incomplete spin transition, which is in line with the magnetic and ESR data. The similar line widths of the two doublets suggest that the rate of interconversion between the low-spin and residual high-spin molecules is close to zero.

The temperature dependence of μ_{Fe} for three pyrazole adducts, containing different anions (viz. $[Fe(salen)(pyz)_2]Y$, $Y = ClO_4^-$, BF_4^-, BPh_4^-), is shown in Figure 6. An anion dependence of the $^6A_1 \rightleftharpoons {}^2T_2$ crossover similar to that described above for the analogous imidazole complexes appears to be present. The spin transitions for the ClO_4^- and BF_4^- complexes are both incomplete as judged by the relatively high value of μ_{Fe} at low temperatures (2.51 and 2.32 μ_B, respectively) and by the appearance of signals near $g = 4.3$ in the ESR spectra.

Crystal and Molecular Structures of $[Fe(salen)(imd)_2]Y$ Complexes at 295 K ($Y = ClO_4^-$, PF_6^-, BF_4^-) and 120 K ($Y = ClO_4^-$). It is evident from the above magnetic and spectral discussion that a wide variation in spin state can be induced in the *trans*-[Fe-

Table VI. Iron Atom Environments in $[Fe(salen)(imd)_2]Y$ (Y = ClO_4^- at 120 K (**1a**), ClO_4^- at 295 K (**1b**), BF_4^- (**2**), PF_6^- (**3**))[a]

	r	N(18)	O(21)	N(28)	N(31)	N(41)
			Compound **1a**			
O(11)	1.885 (4)	93.4 (2)	87.3 (2)	177.5 (2)	89.4 (2)	91.2 (2)
N(18)	1.905 (4)		178.0 (2)	84.5 (2)	89.8 (2)	91.7 (2)
O(21)	1.921 (4)			94.7 (2)	88.3 (2)	90.2 (2)
N(28)	1.921 (5)				89.2 (2)	90.3 (2)
N(31)	1.990 (5)					178.3 (2)
N(41)	1.993 (4)					
			Compound **1b**			
O(11)	1.885 (4)	89.6 (2)	100.8 (2)	169.3 (2)	92.3 (2)	92.2 (2)
N(18)	2.051 (4)		169.1 (2)	79.7 (2)	86.6 (2)	91.2 (2)
O(21)	1.917 (4)			90.0 (2)	89.5 (2)	91.8 (2)
N(28)	2.083 (4)				87.9 (2)	87.2 (2)
N(31)	2.141 (5)					175.0 (2)
N(41)	2.151 (5)					
			Compound **2**			
O(11)	1.897 (6)	90.1 (3)	99.6 (3)	169.8 (3)	91.7 (3)	93.0 (3)
N(18)	2.055 (7)		169.0 (3)	79.7 (3)	85.3 (3)	91.9 (3)
O(21)	1.906 (6)			90.5 (3)	89.3 (3)	92.6 (3)
N(28)	2.089 (7)				87.7 (3)	87.2 (3)
N(31)	2.117 (8)					174.6 (3)
N(41)	2.128 (7)					
			Compound **3**			
O(11)	1.913 (5)	88.0 (2)	107.2 (2)	164.4 (2)	89.1 (2)	92.1 (2)
N(18)	2.146 (5)		164.7 (2)	76.8 2)	90.0 (2)	88.8 (2)
O(21)	1.894 (5)			88.2 (2)	91.7 (2)	89.2 (2)
N(28)	2.125 (7)				87.6 (2)	91.0 (2)
N(31)	2.153 (5)					178.3 (2)
N(41)	2.153 (5)					

[a] The entries in the first column of data are the iron–ligand distances, $r_{Fe-O,N}$ (Å). Other entries are the angles (deg) subtended by the relevant atoms at the head of the row and column.

Table VII. Ligand Geometries: Distances (Å)[a]

	1a	**1b**	**2**	**3**
		Quadridentate Ligand		
O(1)–C(1)	1.303 (6), 1.321 (6)	1.317 (7), 1.322 (6)	1.31 (1), 1.33 (1)	1.321 (8), 1.314 (9)
C(1)–C(2)	1.420 (8), 1.424 (8)	1.398 (8), 1.407 (8)	1.43 (1), 1.42 (1)	1.403 (11), 1.397 (10)
C(1)–C(6)	1.428 (7), 1.432 (7)	1.416 (9), 1.419 (8)	1.40 (2), 1.43 (1)	1.403 (9), 1.407 (11)
C(2)–C(3)	1.391 (9), 1.376 (8)	1.388 (10), 1.360 (9)	1.48 (2), 1.36 (1)	1.364 (11), 1.376 (13)
C(3)–C(4)	1.406 (10), 1.399 (9)	1.343 (14), 1.403 (9)	1.33 (2), 1.37 (1)	1.379 (11), 1.382 (13)
C(4)–C(5)	1.371 (9), 1.368 (9)	1.402 (10), 1.368 (10)	1.35 (2), 1.35 (1)	1.388 (13), 1.350 (12)
C(5)–C(6)	1.407 (8), 1.412 (8)	1.406 (9), 1.384 (8)	1.41 (2), 1.44 (1)	1.381 (10), 1.417 (11)
C(6)–C(7)	1.438 (8), 1.428 (8)	1.429 (8), 1.472 (9)	1.44 (1), 1.41 (1)	1.443 (11), 1.434 (10)
C(7)–N(8)	1.288 (7), 1.288 (7)	1.279 (8), 1.266 (7)	1.32 (1), 1.29 (1)	1.274 (9), 1.296 (9)
N(8)–C(9)	1.472 (7), 1.473 (8)	1.474 (7), 1.473 (8)	1.47 (1), 1.46 (1)	1.442 (9), 1.455 (9)
C(9)–C(9)	1.540 (8)	1.518 (9)	1.54 (1)	1.52 (1)
		Imidazole Ligands		
N(1)–C(2)	1.324 (7), 1.333 (7)	1.307 (7), 1.303 (7)	1.32 (1), 1.28 (1)	1.318 (8), 1.316 (9)
N(1)–C(5)	1.382 (7), 1.376 (7)	1.365 (7), 1.374 (7)	1.36 (1), 1.38 (1)	1.365 (12), 1.378 (9)
C(2)–N(3)	1.341 (8), 1.344 (7)	1.345 (8), 1.343 (8)	1.34 (1), 1.35 (1)	1.333 (11), 1.307 (10)
N(3)–C(4)	1.374 (8), 1.371 (7)	1.343 (8), 1.365 (8)	1.37 (1), 1.37 (1)	1.348 (13), 1.349 (10)
C(4)–C(5)	1.350 (8), 1.383 (8)	1.353 (9), 1.375 (9)	1.37 (1), 1.32 (1)	1.331 (9), 1.373 (11)
O(1)···N(8)	2.758 (6), 2.826 (6)	2.776 (6), 2.830 (6)	2.80 (1), 2.84 (1)	2.801 (8), 2.825 (7)
O(1)···O(1)	2.627 (6)	2.928 (5)	2.904 (8)	3.064 (7)
N(8)···N(8)	2.573 (6)	2.649 (6)	2.66 (1)	2.652 (9)
H(42)···O(21)			2.6_4	(2.5_6[b]), 2.5_6

[a] The two values for each entry are for components 1 and 2 of the quadridentate ligand or imidazoles 3 and 4 as appropriate. [b] H(32)···O(11).

$(salen)(imd)_2]^+$ species by appropriate combination of anion and temperature, and the system lends itself well to study by single-crystal X-ray diffraction methods. The hexafluorophosphate **3**, high spin down to a very low temperature, the tetrafluoroborate **2**, and perchlorate **1**, with doublet and sextet states of similar energies, both substantially populated at room temperature but diminishing to almost purely low-spin behavior at liquid-nitrogen temperatures (particularly in the case of the perchlorate), provide a wide spectrum of behavior for study and accordingly were used in the present work, **1** at both room temperature (labeled **1b**) and 120 K (labeled **1a**) and **2** and **3** at room temperature. In addition, these complexes have the advantage of presenting essentially simple structures with one cation/anion pair per asymmetric unit in each case and, in spite of anions with a predisposition toward disorder, with disorder only occurring in the hexafluorophosphate, in which two anion components with equal populations may be deconvoluted.

Bond distances and angles in the Fe atom environments of the complexes are given in Table VI. The ligand and anion geometries are given in Tables VII–IX, and equatorial iron environment planes are given in Table X. The molecular structures of **1b** and **3** are displayed in Figure 7.

The lattice arrays of **1a,b** and **2** are essentially isostructural; at room temperature the differences in cation geometry of **1b** and

Table VIII. Ligand Geometries: Angles (deg)[a]

	1a	1b	2	3
		Quadridentate Ligand		
Fe-O(1)-C(1)	123.7 (3), 125.7 (3)	128.3 (4), 130.4 (3)	126.6 (6), 130.7 (5)	132.9 (5), 133.1 (4)
O(1)-C(1)-C(2)	118.1 (5), 117.4 (5)	118.7 (6), 117.9 (5)	117.7 (9), 119.5 (8)	118.3 (6), 118.4 (7)
O(1)-C(1)-C(6)	124.6 (5), 124.3 (5)	122.1 (5), 124.8 (5)	125.0 (9), 122.8 (8)	123.9 (7), 123.5 (6)
C(2)-C(1)-C(6)	117.3 (5), 118.3 (5)	119.1 (5), 117.3 (5)	117.3 (9), 117.7 (8)	117.6 (6), 118.0 (7)
C(1)-C(2)-C(3)	121.2 (5), 120.2 (5)	120.6 (7), 121.2 (5)	115 (1), 121.3 (9)	121.8 (7), 121.0 (8)
C(2)-C(3)-C(4)	120.6 (6), 121.8 (5)	120.7 (7), 121.4 (6)	126 (1), 122.2 (10)	120.4 (8), 120.4 (8)
C(3)-C(4)-C(5)	118.9 (6), 118.9 (5)	121.0 (7), 117.9 (6)	119 (1), 118.8 (9)	118.8 (7), 120.5 (8)
C(4)-C(5)-C(6)	122.0 (6), 122.1 (5)	119.8 (7), 122.3 (6)	120 (1), 122.4 (9)	121.5 (7), 120.4 (8)
C(1)-C(6)-C(5)	119.8 (5), 118.7 (5)	118.8 (5), 119.8 (5)	123.6 (9), 117.3 (9)	119.8 (7), 119.6 (6)
C(1)-C(6)-C(7)	121.9 (5), 123.7 (5)	124.1 (5), 123.0 (5)	123.6 (9), 124.5 (9)	122.9 (6), 123.6 (6)
C(5)-C(6)-C(7)	118.2 (5), 117.6 (5)	117.0 (6), 117.2 (5)	112.8 (10), 118.1 (9)	117.2 (6), 116.8 (7)
C(6)-C(7)-N(8)	123.6 (5), 125.4 (5)	124.9 (5), 124.9 (5)	123.9 (9), 126.7 (9)	127.4 (6), 125.9 (7)
Fe-N(8)-C(7)	126.3 (4), 126.1 (4)	124.8 (3), 126.7 (4)	124.2 (6), 124.4 (7)	124.1 (5), 124.6 (5)
C(7)-N(8)-C(9)	121.6 (4), 119.9 (5)	122.8 (4), 119.1 (5)	122.0 (8), 121.9 (8)	121.3 (6), 119.9 (7)
Fe-N(8)-C(9)	111.9 (3), 113.9 (3)	112.3 (3), 114.1 (3)	113.8 (6), 113.7 (5)	114.6 (4), 115.5 (5)
N(8)-C(9)-C(9′)	106.0 (4), 105.9 (4)	107.9 (5), 107.9 (5)	106.6 (8), 109.3 (8)	109.6 (5), 108.4 (7)
		Imidazole Ligands		
Fe-N(1)-C(2)	126.3 (4), 122.9 (3)	125.5 (4), 122.4 (4)	127.4 (6), 122.3 (6)	125.8 (6), 125.2 (5)
Fe-N(1)-C(5)	126.5 (4), 130.8 (4)	127.6 (4), 130.9 (4)	126.8 (6), 133.1 (6)	128.7 (4), 128.9 (4)
C(2)-N(1)-C(5)	107.2 (5), 106.3 (5)	106.8 (5), 106.3 (5)	105.8 (8), 104.3 (8)	105.2 (6), 106.0 (6)
N(1)-C(2)-N(3)	109.5 (5), 111.3 (5)	110.1 (5), 111.7 (5)	111.3 (8), 112.9 (8)	110.6 (8), 110.8 (6)
C(2)-N(3)-C(4)	108.5 (5), 107.4 (4)	107.8 (5), 107.4 (5)	107.1 (8), 105.5 (8)	107.8 (6), 109.8 (6)
N(3)-C(4)-C(5)	106.3 (5), 106.5 (5)	106.7 (5), 105.8 (5)	106.0 (9), 106.0 (8)	106.4 (8), 105.1 (6)
N(1)-C(5)-C(4)	108.6 (5), 108.5 (5)	108.5 (5), 108.8 (5)	109.7 (8), 111.2 (9)	110.1 (8), 108.4 (6)

[a] The two values for each entry are for components 1 and 2 of the quadridentate ligand or imidazoles 3 and 4 as appropriate.

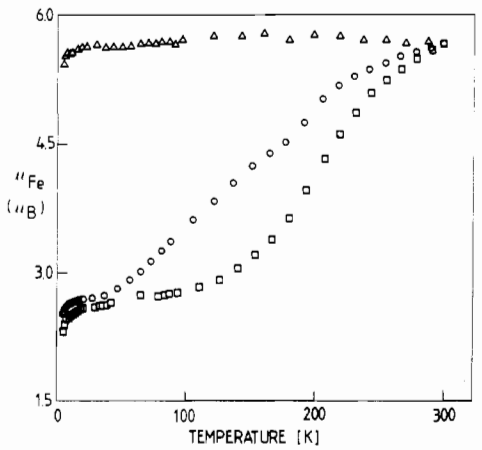

Figure 6. Magnetic moments vs. temperature for $[Fe(salen)(pyz)_2]Y$: (△) Y = BPh_4^-; (○) Y = ClO_4^-; (□) Y = BF_4^-.

2, where significant, are only trivial, in keeping with the minor difference in room-temperature magnetic behavior. Anion thermal vibration envelopes are similar, differing essentially only in magnitude, and accordingly, further discussion of **2** will be subsumed under that of **1b**. The cation conformation of **1b** is preserved in **1a** on cooling; by contrast, in spite of the rather similar room-temperature magnetic moment, this is not the case in **3**, the lattice of which is not isostructural with the others. In the cation of **3** the dihedral angle between the two essential coplanar, conjugated ligand halves is 1.4°; the bridging carbon atoms C(9) lie with deviations to either side of the central coordination plane, with deviations from their respective aromatic planes of −0.31, 0.25 Å; the iron atom deviations from these planes are 0.13, −0.14 Å. By contrast, in the cation of **1b** (and **2**), substantial angles between the two half-ligand aromatic planes are observed (22.5° (21.3°)); one bridge atom (C(19)) lies well to one side of the coordination plane, with C(19,29) deviations from their respective aromatic planes being 0.08, 0.32 Å (**1b**) (and 0.11, 0.25 Å (**2**)), while the iron atom deviates grossly from one ligand plane (section 1) relative to the other (0.60, 0.14 Å in **1b**; 0.63, 0.07 Å in **2**). The five-membered FeN_2C_2 ring has thus essentially adopted an envelope conformation, in **1b** and **2** with C(9,section 2) as the deviant atom, the distortion and torsion of the ring being reflected in the relative disposition of the halves of the ligands. In spite

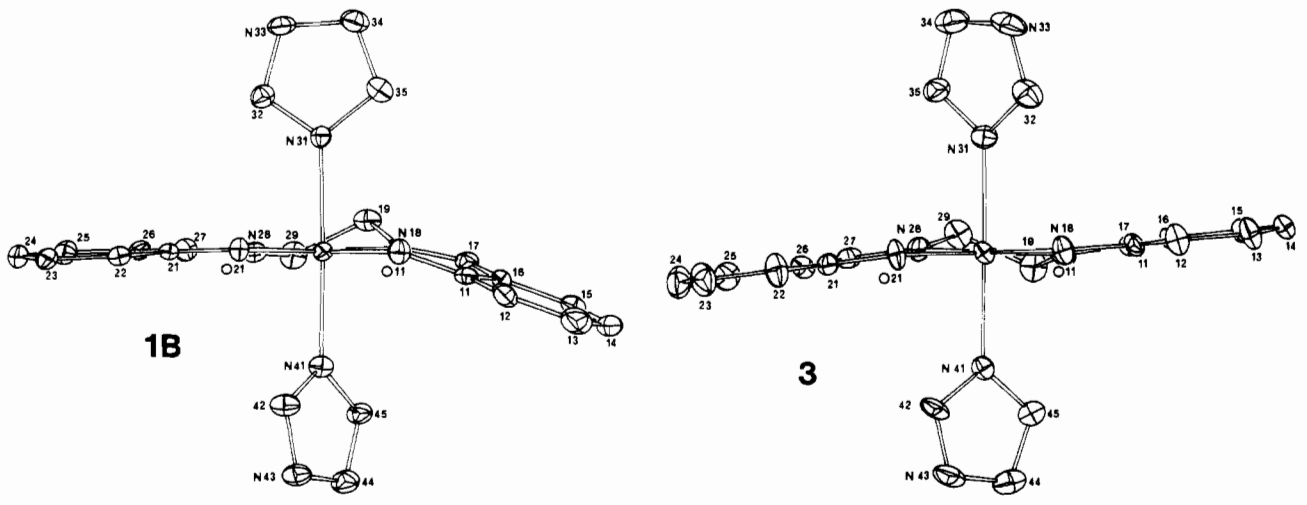

Figure 7. Molecular structures (ORTEP diagrams) of $[Fe(salen)(imd)_2]ClO_4$ (**1b**) and $[Fe(salen)(imd)_2]PF_6$ (**3**) showing the different salen conformations.

Table IX. Anion Geometries[a]

Compound **1a**

	r_{Cl-O}	O(2)	O(3)	O(4)
O(1)	1.448 (5)	109.6 (3)	109.0 (3)	109.0 (3)
O(2)	1.431 (5)		110.0 (3)	109.7 (3)
O(3)	1.438 (5)			109.5 (3)
O(4)	1.448 (5)			

Compound **1b**

	r_{Cl-O}	O(2)	O(3)	O(4)
O(1)	1.434 (6)	110.6 (3)	110.9 (4)	106.1 (3)
O(2)	1.390 (5)		109.3 (3)	111.0 (4)
O(3)	1.406 (5)			109.0 (3)
O(4)	1.427 (6)			

Compound **2**

	r_{B-F}	F(2)	F(3)	F(4)
F(1)	1.40 (2)	109.9 (10)	108.7 (11)	102.8 (9)
F(2)	1.33 (1)		115.6 (9)	110.5 (10)
F(3)	1.32 (1)			108.5 (10)
F(4)	1.38 (1)			

Compound **3**

	r_{P-F}	F(2)	F(3)	F(4)	F(5)	F(6)
F(1)	1.535 (7)	86.2 (5)	177.9 (5)	93.1 (6)	86.4 (5)	89.1 (5)
F(2)	1.534 (9)		95.9 (6)	87.5 (6)	166.7 (7)	94.0 (7)
F(3)	1.556 (8)			87.0 (6)	91.5 (6)	90.8 (6)
F(4)	1.583 (13)				81.9 (6)	177.4 (6)
F(5)	1.571 (10)					96.9 (7)
F(6)	1.481 (12)					
	$r_{P-F'}$	F(2′)	F(3′)	F(4′)	F(5′)	F(6′)
F(1′)	1.55 (1)	97.1 (8)	173.3 (7)	81.1 (9)	92.6 (9)	84.7 (9)
F(2′)	1.51 (2)		83.6 (8)	84.7 (9)	165.1 (8)	88.6 (9)
F(3′)	1.50 (1)			105.7 (9)	88.1 (9)	88.6 (9)
F(4′)	1.50 (1)				85.6 (10)	163.3 (13)
F(5′)	1.46 (2)					103.7 (10)
F(6′)	1.42 (1)					

[a] The entries in the first column of data are the central atom–peripheral atom distances (Å). Other entries are the angles (deg) subtended by the relevant atoms at the head of the row and column.

Table X. Equatorial Iron Environment Planes[a]

	1a	**1b**	**2**	**3**
χ^2	101.7	272.5	184.9	172.8
δ(Fe)	0.003	0.003	0.007	−0.002
δ(O(11))	−0.019	0.006	−0.004	0.042
δ(N(18))	−0.033	−0.065	−0.088	−0.044
δ(O(21))	−0.025	−0.049	−0.070	−0.025
δ(N(28))	−0.024	0.018	0.009	0.062
δ(C(19))	−0.540	−0.558	−0.551	−0.292
δ(C(29))	0.083	0.090	0.100	0.332
θ_1	21.1	21.2	21.6	6.2
θ_2	1.8	2.8	1.8	6.8

[a] Atom deviations (Å) from a least-squares plane defined by Fe, O(11,21), N(18,28) are given, together with the deviations of C(19,29) and the dihedral angles θ_1, θ_2 (deg) to benzene ring planes C(11–16) and C(21–26), respectively.

of the magnetic moment being similar to that of **3** for these two species, it is not evident from the structure determination to what extent the conformational difference between **1b** and **3** is a product of dimensional change correlating with magnetic moment, or simply packing forces. Although the latter must be the ultimate determinant of the overall array, and the relative disposition of the ligand halves, it is of interest to note that the magnetic moment of **3** is insensitive to change in temperature, suggesting that the ligand disposition adopted is such that the geometry about the metal atom may be more strongly predetermined than in **1** and **2**; i.e., the resulting geometrical constraint of a planar ligand produces an incapacity to adapt to incipient spin-state change so that the complex is essentially "locked" in the high-spin form. In consequence, it might be predicted that other essentially temperature-dependent "high-spin" salts of this anion should also have central FeN_2C_2 rings adopting the "meso" rather than "envelope" conformations.

In consequence, some rather surprising differences are found in metal atom environments. Throughout all systems metal–oxygen distances are essentially constant, regardless of change of spin state/temperature/ligand conformation. The O···O distance and the Fe–O–C angles are susceptible to wide variations, up to 0.44 Å and 9.2°, respectively (see Tables VII and VIII), whereas some other parameters of "bite" between various coordinating atoms are much less susceptible; O···N and N···N cover a range of up to ~0.1 Å. Interestingly, in **1** and **2**, where differences in interaction of the ligand halves with the iron atom are suggested by the great disparity in iron atom deviation from the ligand plane, the difference in O···N for the ligand halves can be ~0.08 Å (**1a**).

In spite of the similarity in N···N distances in **1b**, **2**, and **3** and in their magnetic moments, the difference in the associated Fe–N distances is rather surprising, those of **3** (mean 2.13_6 Å) being ~0.07 Å longer than those of **1b** and **2**, even though there are larger iron atom deviations from the two ligand half-planes in the latter. In the latter, the distances associated with the halves of the ligand are consistently different, the longer of the two ($\sim 2.08_5$ Å) correlating with the less deviant iron atom, a result perhaps surprising in view of expectations about bonding strength. On passing to the low-temperature form of **1**, Fe–N contracts dramatically as expected for the low-spin state; there is little associated change in the dihedral angle between the ligand halves or in iron atom deviations from these, in spite of the considerable changes in "bite" parameters.

Iron–imidazole nitrogen distances are similar in all high-magnetic-moment species, lying at or approaching 2.15 Å; again, on passing to the low-temperature form of **1**, this distance shortens dramatically to 1.99 Å. In the PF_6^- salt **3**, with the meso-bridge

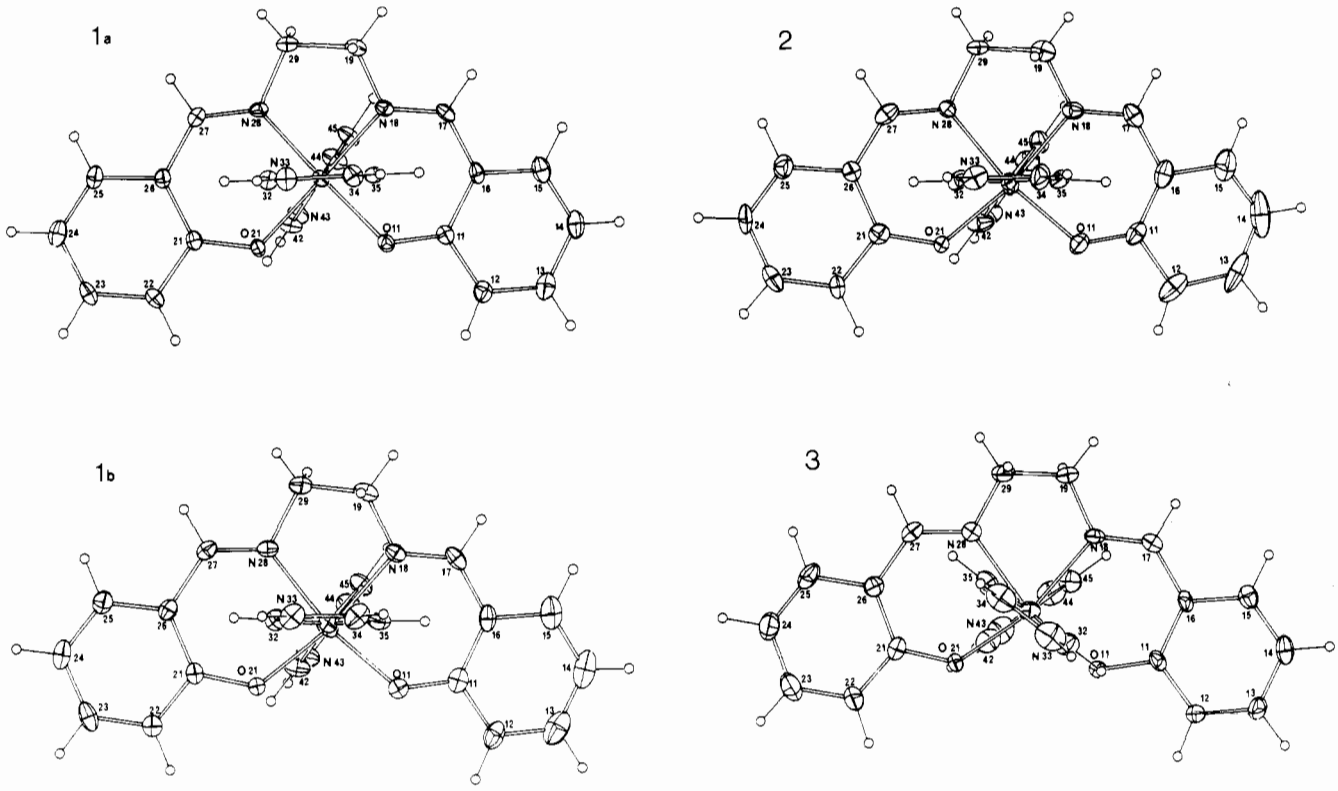

Figure 8. Projections of the cations of **1a,b**, **2**, and **3** down the imidazole N(31)–N(41) direction (imidazole 3 nearest the reader). Non-hydrogen atoms are shown as 20% thermal ellipsoids except for **1a**, which are 50%; hydrogen atoms have an arbitrary radius of 0.1 Å.

conformation for the quadridentate ligand, the imidazole ligands are both approximately coplanar with one of the *trans*-O–Fe–N systems of the quadridentate, and each imidazole N(n3) lies disposed approximately above an oxygen atom; cation symmetry thus approaches *2* (see Figure 8). In the remaining systems, imidazole 4 retains this disposition and lies on the opposite site of the quadridentate coordination plane to the envelope deviation of C(19), contained in the obtuse angle (<180°) between the two half-ligand planes. Imidazole 3 is rotated about the bond to the metal atom by ~135°, so as to take up a disposition approximately coplanar with the long cation axis little affected by change of spin state. The disposition of the ligands in the PF_6^- salt **3** exhibits close quadridentate O···H(n2) contacts of 2.5$_6$ Å; these are retained for imidazole 4 in the other compounds at ~2.6 Å, but not for imidazole 3. It is not inconceivable that the imidazole H···O interactions may have some influence on the crystal field at the metal; there are significant differences in Fe–O(11,21) in both **1a** and **1b**, where Fe–O(11), with no hydrogen contact to the oxygen, is shorter than Fe–O(21), where such contact is observed; this difference is less pronounced in **2**. The differences of 0.036, 0.032, and 0.009 Å in any case are not greatly different from the 0.019-Å difference found in **3**, where the interactions are symmetrical to both oxygens. Nevertheless, it is of interest to observe that, for imidazole 3 in **1a,b** and **2** angles Fe–N(1)–C(2,5) are symmetrical, or almost so, but a pronounced asymmetry in these angles is observed for the hydrogen-bonded ligand 4, with Fe–N(1)–C(2) less than Fe–N(1)–C(5), in keeping with the direction of the interaction. In **3**, *both* imidazoles are tilted in this direction.

A recent variable-temperature structure determination on the $Fe^{III}N_4O_2$ complex $[Fe(3EtO\text{-}salAPA)_2]ClO_4\cdot C_6H_6$, made by Strouse, Hendrickson, and co-workers,[8] is of interest in relation to the present study. This bis(tridentate) compound displays a gradual, complete spin-crossover transformation with magnetic and spectral features similar to those of $[Fe(salen)(imd)_2]ClO_4$. The changes in Fe–O and Fe–N(imine) distances as a function of temperature and spin state are similar for the two complexes. The equatorial O_2N_2 donor set in the $(salAPA)_2$ complex contains a trans donor atom rearrangement compared to the cis arrangement in the salen compound. Interestingly, a change in the space group of the salAPA complex occurring between 298 and 175 K, due to an order–disorder transformation (at 180 K), apparently has no influence on the magnetic and spectroscopic data. There is, of course, no such space group change in the present case.

The other structural work on spin-crossover Fe^{III} complexes relevant to the present study is that by Scheidt and co-workers[17-19] on six-coordinate porphyrins of type $[Fe(OEP)(L)_2]ClO_4$, where L = 3Cl-py or 2Me-imd. The key features to emerge from studies on crystalline samples are generally similar to those observed here in the Schiff-base compounds. Two crystalline forms of the 3Cl-py adduct were isolated, each with different magnetic properties and spin ground states.[17,18] The spin-state differences in these forms and in the 2Me-imd analogue[19] were ascribed to axial ligand orientation effects, which in turn were brought about by solid-state packing effects. More subtle effects were also described in the case of the 2Me-imd complex, similar to those described above for the present imd species, involving nonbonded contacts between the (unsubstituted) α-carbon of the 2Me-imd rings and the porphyrin core.

Effects of Varying the In-Plane Quadridentate Ligand Imidazole Adducts, $[Fe(chelate)(imd)_2]BPh_4$. The temperature dependence of μ_{Fe} for the 3MeO-salen complex is dramatically different from that displayed by the salen derivative (Figure 9). At low temperatures the moment is reasonably temperature-independent with a value of ca. 2.0 μ_B, suggestive of a low-spin ground state. Above 70 K μ_{Fe} increases quite rapidly to ca. 4.1 μ_B at 150 K and then more slowly. Although the value of μ_{Fe} above 150 K is close to that expected for an intermediate-spin ($S = {}^3/_2$) Fe^{III} complex, the Mössbauer spectrum at 295 K (Figure 10) shows the presence of both high-spin and low-spin molecules (Table XI). There is some hint of a third weak outer doublet at 295 K, but this is not observed at lower temperatures. The observation of distinct doublets due to high- and low-spin Fe^{III} at high temperatures means that the rate at which individual molecules interchange their spin states is less than the inverse of the ^{57}Fe Mössbauer time scale. This contrasts with $[Fe(salen)(imd)_2]ClO_4$, for which only a single doublet is observed. The presence of both a high-temperature and low-temperature plateau in the μ_{Fe} values indicates that the transitions to high and low spin are incomplete, an observation supported by the Mössbauer data. Aging the sample

Table XI. Mössbauer Spectral Parameters for Crossover [Fe(Schiff base)$(L)_2$]BPh_4 Complexes

complex	T, K	δ, mm s^{-1}	ΔE_Q, mm s^{-1}	% area	spin state
[Fe(3MeO-salen)$(imd)_2$]BPh_4	295[a]	0.15	2.38	28.6	$^1/_2$
		0.33	0.90	66.0	$^5/_2$
	77	0.18	2.47	67.3	$^1/_2$
		0.42	0.87	32.7	$^5/_2$
	4.2	0.20	2.44	64.1	$^1/_2$
		0.42	0.86	35.9	$^5/_2$
	4.2[b]	0.19	2.46	73.4	$^1/_2$
		0.42	0.88	26.6	$^5/_2$
[Fe(3EtO-salen)$(imd)_2$]BPh_4	300	0.31	1.38	100.0	$^5/_2$
	4.2	0.20	2.26	100.0	$^1/_2$
[Fe(acen)(*N*-Me-imd$)_2$]BPh_4	77	0.11	2.46	100.0	$^1/_2$
	4.2[c]	0.20	2.58	57.0	$^1/_2$
		0.27	2.43	43.0	$^1/_2$

[a] The fit shown in Figure 10 also contains ~5% of a doublet with very large quadrupole splitting, which is probably just due to base-line scatter. [b] Remeasured after 1 year. [c] Two doublets, as shown, gave a better fit than one doublet.

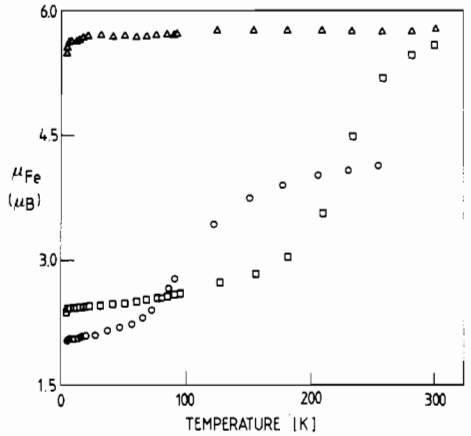

Figure 9. Magnetic moment vs. temperature: (△) [Fe(salen)$(imd)_2$]BPh_4; (□) [Fe(3EtO-salen)$(imd)_2$]BPh_4 (○) [Fe(3MeO-salen)$(imd)_2$]BPh_4.

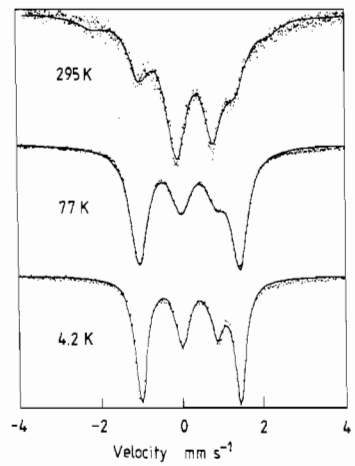

Figure 10. Zero-field Mössbauer spectra of [Fe(3MeO-salen)$(imd)_2$]BPh_4 at 295, 77, and 4.2 K.

for 12 months leads to only very minor changes in the 4.2 K Mössbauer spectrum. As in the case of [Fe(salen)$(imd)_2$]BPh_4, the 3MeO-salen complex shows a lower percentage of low-spin molecules at 4.2 K, as judged by the area of the Mössbauer doublets, compared to that deduced from the susceptibility data on account of differing Debye–Waller factors for the low- and high-spin states. The present susceptibility data on the 3MeO-salen complex show only slight differences to those reported by Nishida et al.[4] in the range 77–300 K.

The magnetic moment of [Fe(3EtO-salen)$(imd)_2$]BPh_4 is much more temperature-dependent than that of the 3-methoxy compound, decreasing from 5.58 μ_B at 298 K to 2.38 μ_B at 4.2 K. The latter value is a little higher than anticipated for a complete spin transition and is suggestive of some residual high-spin character, although there is no evidence for any high-spin doublet in the 4.2 K Mössbauer spectrum. The room-temperature Mössbauer spectrum shows only a high-spin doublet in agreement with the magnetic data (Table XI).

Table XII. Zero-Field Splitting (ZFS) Parameters for $S = {}^5/_2$ Complexes[a,b]

complex	D, cm^{-1}	E, cm^{-1}
[Fe(salen)$(imd)_2$]PF_6	0.6	0.1
[Fe(salen)(5Cl-*N*-Me-imd$)_2$]ClO_4	0.8	0.2
[Fe(saloph)$(imd)_2$]ClO_4	0.9	0.3
[Fe(3MeO-salen)(*N*-Me-imd$)_2$]ClO_4	1.0	0.3
[Fe(3MeO-salen)(*N*-Me-imd$)_2$]BPh_4	0.3	0.1

[a] Best-fit values obtained as in ref 29 with use of rhombic $S = {}^5/_2$ spin Hamiltonian. [b] Estimated errors: D, ±0.1 cm^{-1}; E, ±0.1 cm^{-1}.

High-spin magnetic moments of ~5.9 μ_B were observed for *N,N'-o*-phenylenebis(salicylaldimine) complexes of type [Fe(saloph)$(imd)_2$]Y (Y = ClO_4^-, BPh_4^-). Fitting of the χ_{Fe}/T data for Y = ClO_4^- to a rhombic spin Hamiltonian yields the following values of the ZFS parameters: $D = 0.9 \pm 0.1$ cm^{-1}, $E = 0.3 \pm 0.1$ cm^{-1}.

***N*-Methylimidazole Adducts.** The four complexes of formula [Fe(R-salen)(*N*-Meimd$)_2$]Y, R = H, OMe and Y = BPh_4^-, ClO_4^-, all show μ_{Fe} values of ca. 5.9 μ_B and have ESR g values of 4.3, in line with pure high-spin behavior. This is confirmed by measurements of susceptibility over the temperature range 300–4.2 K, which can be explained solely in terms of a zero-field-split $^6A_1$ ground state. The best-fit ZFS parameter values are collected in Table XII, together with those for other $S = {}^5/_2$ species. D is ≤1 cm^{-1} in all of these high-spin six-coordinate adducts.

The powder ESR spectrum of [Fe(acen)(*N*-Me-imd$)_2$]BPh_4 at 295 K shows a complex pattern with lines at $g \approx 8.4$ and 4, suggestive of a distorted high-spin Fe^{III} complex, together with an intense line near $g \approx 2$ suggesting the presence of low-spin Fe^{III}. Cooling to 77 K results in a much simpler spectrum being observed (Figure 11) with lines at $g = 2.32$, 2.14, and 1.93, typical of $S = {}^1/_2$ Fe^{III} Schiff-base systems, and no evidence for any high-spin lines. The susceptibility measurements, shown in Figure 12, confirm the completeness of the $^6A_1 \rightleftharpoons {}^2T_2$ transition with μ_{Fe} decreasing from 5.23 μ_B at 297 K to 2.0 μ_B at 75 K and below. The χ_{Fe}/T data were fitted to the model developed by Martin et al.,[30] and best-fit parameters of $E(^6A_1 - {}^2T_2) = 340$ cm^{-1}, log $C = 1.49$, and $g = 2.15$ were obtained. The fit was better than that shown in Figure 3, especially in the region of the maximum in χ_{Fe}^{-1}. The room-temperature Mössbauer spectrum of this complex is broad and poorly resolved, and there are no obvious signals due to either high-spin or low-spin Fe^{III}. The spectrum is similar to that reported recently by Oshio et al.[11] for the closely related complex [Fe(acen)(4Me-py$)_2$]BPh_4 in which a rapid electronic relaxation occurs between the $^6A_1$ and $^2T_2$ states. At 77 K a well-resolved doublet is displayed in which the lower velocity line is a little broader and less intense than the higher velocity line.

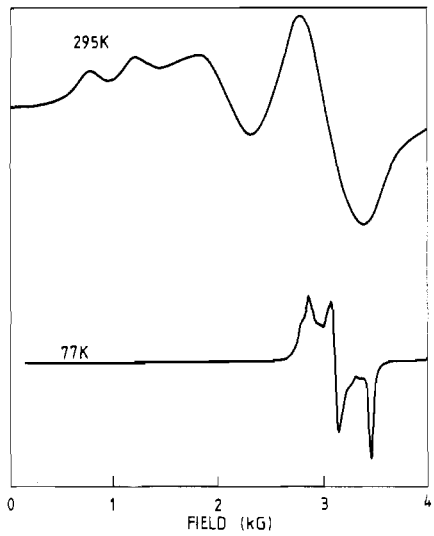

Figure 11. X-Band ESR spectra of polycrystalline [Fe(acen)(*N*-Me-imid)$_2$]BPh$_4$ at 295 and 77 K.

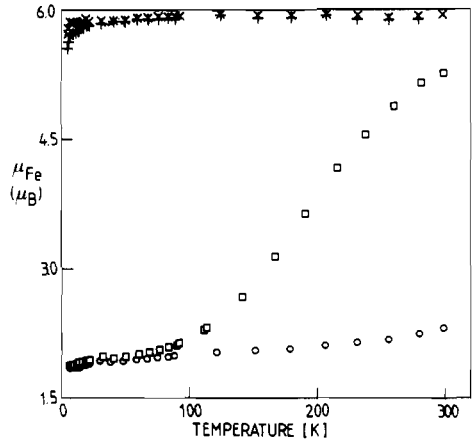

Figure 12. Magnetic moment vs. temperature for *N*-Me-imd adducts: (×) [Fe(3MeO-salen)(*N*-Me-imd)$_2$]BPh$_4$; (+) [Fe(3MeO-salen)(*N*-Me-imd)$_2$]ClO$_4$; (□) [Fe(acen)(*N*-Me-imd)$_2$]BPh$_4$; (○) [Fe(benzacen)(*N*-Me-imd)$_2$]BPh$_4$.

The δ and ΔE_Q values (Table XI) are typical of the $S = {}^1/_2$ ground state. At 4.2 K the spectrum appears as a simple doublet. However, attempts to fit this by using a single Lorentzian doublet failed, suggesting the presence of two doublets, the isomer shift and quadrupole splitting of which are both typical of $S = {}^1/_2$ Fe^{III}. It is possible that two distinct Fe^{III} sites are present in this complex with slightly different geometries, a phenomenon recently observed by Zelentsov et al.[16] in structural studies on thiosemicarbazone-Schiff-base spin-crossover systems. It is not possible to explain the complicated 295 K ESR spectrum in terms of a simple mixture of high-spin and low-spin molecules. It is possible that, in the solid state, relaxation and/or exchange interactions are responsible for the unusual appearance associated with the low-field signals. An alternative explanation is that the relaxation between the high-spin and low-spin states is extremely rapid, $\sim 10^{-10}$ s, giving an "averaged" spectrum.

The related complex [Fe(benzacen)(*N*-Me-imd)$_2$]ClO$_4$ has a room-temperature moment of 2.26 μ_B, which decreases to 2.1 μ_B at 120 K and then remains essentially constant in a manner typical of low-spin systems. The ESR spectra at both 77 and 300 K show only lines due to $S = {}^1/_2$ Fe^{III} (g = 2.35, 2.13, 1.996). However, a slight curvature in the χ_{Fe}^{-1}/T plot suggests some possible interaction with the $^6A_1$ state.

Summary

Despite the range of available compounds being limited by both the inability to obtain adducts containing sterically hindered imidazoles and the production of monobase rather than dibase adducts in some cases, it is possible to make some reasonable conclusions on spin states in solid-state {O$_2$N$_4$} Schiff-base systems of general type [Fe(Schiff base)L$_2$]Y.

(i) In general, we note that subtle variations in all components of the complex, i.e. O$_2$N$_2$ chelate, Lewis base (L), and counterion (Y), can lead to dramatic changes in spin state, encompassing pure high spin, pure low spin, and high-spin ⇌ low-spin crossover. Clearly, this combination of {O$_2$N$_4$} donor atoms produces an overall ligand field close to the crossover point as has been found in related {N$_6$} porphyrin adducts.[17-19,31]

(ii) The counterion Y influences spin state in a similar pattern in [Fe(salen)(imd)$_2$]Y and [Fe(salen)(pyz)$_2$]Y species. Thus, the PF_6^- and BPh_4^- salts are high spin, while ClO_4^- and BF_4^- undergo spin crossover. Detailed X-ray crystallographic studies on the Y = ClO_4^-, BF_4^-, PF_6^- salts of the imidazole adduct suggest that structural features in the Fe^{III} complex are probably responsible for spin-state differences. In particular, the planar salen conformation, containing a "meso" FeN$_2$C$_2$ ring, leads to the PF_6^- complex being "locked in" to the high-spin form. This is probably why the saloph structure, with a more rigid planar arrangement than salen, is also high-spin. The nonplanar salen "umbrella" conformation, incorporating an envelope FeN$_2$C$_2$ ring, found in the ClO_4^- and BF_4^- structures, leads to the Fe^{III} center being more susceptible to spin-state change. More subtle structural effects that could influence the ligand field at the metal were observed as hydrogen-bonding interactions between the phenolate O atom of the salen and the C–H hydrogen disposed between the nitrogen atoms of imidazole. These lead to small changes in Fe–O bond length and to Fe–imidazole tilt angle with differences in detail being observed between the high-spin and spin-crossover systems. The low-temperature crystal structure of the ClO_4^- salt showed that there is a smooth change in the refined structural parameters with temperature. There is no abrupt phase change occurring. The structural changes correlate well with the magnetic and spectral changes occurring during the gradual crossover transition.

Counterion dependencies of spin-crossover transitions, particularly in relation to the spin-state interconversion rates, have also recently been observed in bis(tridentate) Fe^{III} complexes.[9,24]

(iii) The order of the spin-pairing ability of the in-plane quadridentate Schiff-base ligands is saloph < salen < 3EtO-salen < 3MeO-salen < acen < benzacen. This order is rather approximate since it was not possible to keep L and Y constant in all cases studied. While there are some similarities in this order with that found in Co(Schiff-base)L systems,[2] there are also some differences that are probably due to the different displacements from the O$_2$N$_2$ plane experienced by the Co^{II} and Fe^{III} atoms.

(iv) Within the limited variation in axial ligand, L, available to us, the order of spin-pairing ability is imd ≈ pyz > *N*-Me-imd. Comparison with the work of Nishida et al.[4] places py between imd and *N*-Me-imd. Interestingly, the recent data for the monobase adducts of a quinquedentate Schiff-base Fe^{III} complex[12] yields the order py > imd ≈ *N*-Me-imd. However, the presence of a secondary amine N donor atom trans to the Lewis base in the latter series may well influence these small differences in ligand-field effects.

(v) In addition to the influence on the spin-crossover transition exerted by intramolecular and structural features of the type described above, it has been shown recently by Hendrickson,[7,13,14] Gütlich,[32] König,[33] and Sorai and Seki[34] that intermolecular effects in the solid state can also be significant. It is not the intention here to go over theories of cooperativity and domains or nucleation and growth mechanisms since these have been dealt with elsewhere at length. As far as we are able to ascertain, within the limitations of our instrumentation, there does not appear to be any thermal hysteresis occurring in the susceptibilities at the crossover region, thus implying a continuous type spin transition.[32] However, the

(31) Gregson, A. K. *Inorg. Chem.* **1981**, *20*, 81.
(32) Gütlich, P. *Struct. Bonding (Berlin)* **1981**, *44*, 83.
(33) König, E.; Ritter, G.; Kulshreshtha, S. K.; Nelson, S. M. *J. Am. Chem. Soc.* **1983**, *105*, 1924.
(34) Sorai, M.; Seki, S. *J. Phys. Chem. Solids* **1974**, *35*, 555.

observation of incomplete spin transitions in a number of the present examples probably results from effects such as grinding of the crystallites or the exact conditions used for synthesis and isolation. Hendrickson[13,14] has explained such effects in terms of some of the Fe^{III} Schiff-base molecules (i.e. a minority domain of particular spin-state) existing in a slightly different crystalline environment to the bulk of the molecules. This could result from crystal defects caused either by mechanical aggravation or more subtle effects such as the presence or absence of trace amounts of solvent molecules. Defects at the domain edge are then capable of influencing the spin transition. It seems to us, however, that it is difficult to adequately explain Mössbauer spectra of the type exhibited by complexes such as $[Fe(salen)(imd)_2]ClO_4$ using domain theory. Because the relaxation time of the high-spin state to the low-spin state is faster than the Mössbauer lifetime ($\sim 10^{-7}$ s), a ^{57}Fe nucleus "sees" an average spin state. In such a situation it is difficult to envisage how a minority domain could interact with a neighboring domain and trigger the spin transition. It is tempting to favor the Ising type random distribution model of König[33] and Gütlich,[32] especially above and below the transition temperature, where the percentage of molecules of the "second" spin state is very small in cases of complete spin transition and larger in incomplete transitions. At the actual crossover region complex electronic interactions are occurring. It is possible that the increase of the minority spin occurs in a much more systematic manner throughout the lattice than implied by the expression "random distribution".

Acknowledgment. We gratefully acknowledge the receipt of grants from the Australian Research Grants Scheme (K.S.M. and A.H.W.) and Monash University Special Research Grants (K. S.M.) in support of this work. We thank Dr. J. D. Cashion, Dr. J. R. Pilbrow, and G. Brain for help with Mössbauer and ESR spectral studies.

Supplementary Material Available: Tables SUP1–4 (non-hydrogen atom anisotropic thermal parameters for $[Fe(salen)(imd)_2]Y$, where Y = ClO_4^- (120 K, **1a**; 295 K, **1b**), BF_4^- (**2**), PF_6^- (**3**), respectively), Tables SUP5 and SUP6 (hydrogen atom parameters for **1a,b** and for **2** and **3**, respectively), Tables SUP7 and SUP8 (least-squares planes for salen ligands and imidazole rings, respectively), and Table SUP9 (microanalytical data) (16 pages); Table SUP10 (structure factors for **1a,b**, **2**, and **3**) (56 pages). Ordering information is given on any current masthead page.

Contribution from the Department of Chemistry, University of Michigan, Ann Arbor, Michigan 48109

Characterization of Mono- and Binuclear Manganese(II) Schiff Base Complexes with Metal–Disulfide Ligation

Dimitri P. Kessissoglou,[1] William M. Butler, and Vincent L. Pecoraro*

Received March 28, 1986

Both mononuclear and binuclear complexes of Mn^{2+} with the Schiff base disulfide ligand *N,N'*-[1,1'-dithiobis(phenylene)]bis(salicylideneaminato) (SALPS) have been synthesized and characterized by electrochemical, magnetic, spectral, and diffraction methods. SALPS acts as a pentadentate ligand using one disulfide sulfur atom and two oxygen and two nitrogen atoms to bind Mn^{2+} forming Mn(SALPS)solvent in donor solvents. $Mn(SALPS)CH_3OH{\cdot}CH_3OH$ crystallizes in the triclinic crystal system, space group $P\bar{1}$, with $Z = 2$, $a = 9.692$ (2) Å, $b = 11.195$ (4) Å, $c = 13.399$ (5) Å, $\alpha = 110.47$ (3)°, $\beta = 94.57$ (3)°, $\gamma = 98.95$(3)°, and $V = 1331.2$ (9) Å^3. The refinement converged with $R = 0.029$ and $R_w = 0.031$ based on 2984 reflections with $I > 3\sigma(I)$. $Mn(SALPS)CH_3OH$ describes a highly distorted octahedral complex with a Mn(II)–S bond length of 2.77 Å. Magnetic and EPR data support the assignment of the manganese oxidation state in this complex. In solvents such as acetonitrile, toluene and methylene chloride, the basic coordination environment is retained; however, solvent is displaced and a bis(μ-phenolato) dimer, $[Mn(SALPS)]_2$, is formed. $[Mn(SALPS)]_2{\cdot}2CH_3CN$ also crystallizes in the triclinic crystal system, space group $P\bar{1}$, with $Z = 2$, $a = 12.311$ (9) Å, $b = 14.818$ (6) Å, $c = 15.141$ (5) Å, $\alpha = 109.99$ (3)°, $\beta = 84.76$ (5)°, $\gamma = 103.33$ (5)°, and $V = 2525$ (3) Å^3. The refinement converged with $R = 0.040$ and $R_w = 0.038$ for 3596 reflections with $I > 3\sigma(I)$. X-ray structural analysis indicates that the manganese ions are separated by 3.30 Å. A complex EPR signal is observed for the dimer in toluene at 90 K, suggesting that the centers are weakly coupled. Analysis of variable-temperature magnetic susceptibility data (1.9–298 K) shows that the manganese ions are antiferromagnetically coupled with $J = -1.88$ (6) cm^{-1} and $g_{av} = 2.00$. Both the monomer and the dimer show completely irreversible cyclic voltammetric traces in DMF and methylene chloride.

Introduction

The synthesis and characterization of manganese coordination complexes are useful toward the understanding of the structure and reactivity of manganese sites in biological systems. Besides an apparent role as a metal ion cofactor in certain ATP utilizing reactions,[2] there are a number of essential functions for which manganoenzymes have been implicated. Among these are detoxification enzymes such as superoxide dismutase[3,4] and pseudocatalase,[5] which respectively use superoxide and hydrogen peroxide as substrates. A multinuclear manganese center has been proposed for the active site of the thylakoid-membrane-associated oxygen-evolving complex of photosystem II.[6–8] Recently, an enzyme that displays acid phosphatase activity has been isolated from sweet potatoes.[9] It is believed that this enzyme contains a Mn(III)–S bond.[10,11] This is a fascinating center since it requires the coexistence of a moderate oxidant, Mn(III), with a thiolate residue, a well-established reducing agent. Manganese(III) ethanedithiolate complexes have been characterized crystallographically;[12–14] however, in most cases Mn(III)–thiolates undergo

(1) Present address: Laboratory of Inorganic Chemistry, Aristotelian University of Thessaloniki, Thessaloniki, Greece.
(2) Weissiger, R. A.; Fridovich, I. *J. Biol. Chem.* **1973**, *248*, 3582.
(3) Stallings, W. C.; Pattridge, K. A.; Strong, R. K.; Ludwig, M. L. *J. Biol. Chem.* **1984**, *256*, 10664.
(4) Kono, Y.; Fridovich, I. *J. Biol. Chem.* **1983**, *258*, 13646.
(5) Beyre, W. F., Jr.; Fridovich, I. *Biochemistry* **1985**, *24*, 6460.
(6) Radmer, R.; Cheniae, G. *Primary Processes of Photosynthesis*; Barber, J., Ed.; Elsevier/North Holland Biomedical: Amsterdam, 1977, 305.
(7) Dismukes, G. C.; Siderer, Y. *Proc. Natl. Acad. Sci. U.S.A.* **1981**, *78*, 274.
(8) de Paula, J. C.; Brudvig, G. W. *J. Am. Chem. Soc.* **1985**, *107*, 2643.
(9) Suguira, Y.; Kawabe, H.; Tanaka, H. *J. Am. Chem. Soc.* **1980**, *102*, 6581.
(10) Suguira, Y.; Kawabe, H.; Tanaka, H.; Fujimoto, S.; Ohara, A. *J. Am. Chem. Soc.* **1981**, *103*, 963.
(11) Kawabe, H.; Sugiura, Y.; Terachi, M.; Tanaka, H. *Biochim. Biophys. Acta* **1984**, *784*, 81.
(12) Seela, J. L.; Huffman, J. C.; Christou, G. *J. Chem. Soc., Chem. Commun.* **1985**, 58.

0020-1669/87/1326-0495$01.50/0